Single-chain magnets and related systems

Claude Coulon[1,2] (✉) • Vivien Pianet[1,2] • Matias Urdampilleta[3] • Rodolphe Clérac[1,2] (✉)

[1] *CNRS, CRPP, UPR 8641, F-33600 Pessac, France.*
coulon@crpp-bordeaux.cnrs.fr, clerac@crpp-bordeaux.cnrs.fr

[2] *Univ. Bordeaux, CRPP, UPR 8641, F-33600 Pessac, France.*

[3] *London Centre for Nanotechnology, University College London, WC1H 0AH, London, UK*

Abstract In this article, the static and dynamic magnetic properties of Single-Chain Magnets and related systems are reviewed. We will particularly focus on the so-called Ising limit for which the magnetic anisotropy energy is much larger than the energy of the intra-chain exchange interactions. The simple regular chain of ferromagnetically coupled spins will be first described. Static properties will be summarized to introduce the dominant role of domain walls at low temperature. The slow relaxation of the magnetization will be then discussed using a stochastic description. The deduced dynamic critical behavior will be analyzed into details to explain the observed magnet behavior. In particular, the effect of applying a magnetic field, often ignored in the literature, will be discussed. Then, more complicated structures including chains of antiferromagnetically coupled magnetic sites will be discussed. Finally, the importance of interchain couplings will be introduced to discriminate between a « real » Single-Chain Magnet and a sample presenting both a magnet-type properties and a three-dimensional antiferromagnetic ordered state at low temperature.

Keywords Magnet • Low-dimensional magnetic systems • Single-chain magnet • Ising model • Slow dynamics of the magnetization • Magnetically ordered phase • Magnetic phase transition

Abbreviations

1-D	one-dimensional
2-D	two-dimensional
3-D	three-dimensional
ac	Alternating-Current
C	Curie constant
dc	Direct-Current
$eiao^-$	1-ethylimidazole-2-aldoximate
H	magnetic field

Hhmp	2-hydroxymethylpyridine
JT	Jahn-Teller
LEA	Local Equilibrium Approximation
LZ	Landau-Zener
M	Magnetization
$miao^-$	1-methylimidazole-2-aldoximate
pao^-	pyridine-2-aldoximate
py	pyridine
$Rsaltmen^{2-}$	*N*,*N*'–(1,1,2,2-tetramethylethylene)-bis(5-Rsalicylideneiminate)
$saltmen^{2-}$	*N*,*N*'–(1,1,2,2-tetramethylethylene)-bis(salicylideneiminate)
SCM	Single-Chain Magnet
SMM	Single-Molecule Magnet
T	Temperature
ξ	correlation length
χ	magnetic susceptibility

1
Introduction

In the last ten years, considerable research effort has been devoted to the synthesis of nanometer scale magnetic systems with the ultimate goal to reduce the size of the magnetic units that store information. Quite generally, such a magnetic unit is able to show a bi-stable behavior at some temperatures and values of the applied magnetic field. A typical magnetic signature of this bistability is a hysteresis loop as shown in Fig. 1.

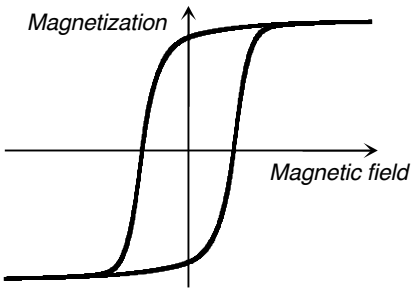

Figure 1. Scheme of the hysteresis effect on the field dependence of the magnetization at a fixed temperature. At zero magnetic field, the magnetization can have two values depending on the magnetic history of the sample. This kind of systems with a hysteresis effect (also called memory effect) is called bi-stable.

Depending of its magnetic history, the sample can be prepared in different metastable states presenting either a positive or negative magnetization. This type of magnetic behavior is commonly observed in materials which present a ferromagnetic or ferrimagnetic long range order, but is also observed in many types of less conventional magnetic systems. The hysteresis loop may have different origin depending on the sample but it always reveals the existence of magnetization slow dynamics, and thus this whole class of materials are called *magnets*. In bulk ordered materials, several magnetic domains are present and displacements of the walls separating these domains are at the origin of the slow relaxation of the magnetization. In samples of smaller size, these domain walls no longer exist and a single magnetic domain is found. In this case, the slow relaxation of the magnetization takes its origin in the existence of an energy barrier due to the magnetic anisotropy. As this energy is proportional to the volume of the sample, there is a size limit down which bistability is no longer observed. This so-called “superparamagnetic limit” imposes a lower limit to the size of the magnetic units used for magnetic storage using conventional materials.

The beginning of the 1990's marked the discovery of Single-Molecule Magnets (SMMs) [1,2,3,4,5,6,7] which gave the hope to store information on a single molecule [8,9,10,11,12,13]. In the 25 years since, numerous SMMs have been discovered and a broad community currently works on new systems with improved magnetic characteristics, although it seems difficult to obtain a magnet behavior at high temperature with such systems. However, SMMs illustrate that the existence of a long range magnetic order is not a necessary condition to obtain a magnet (i.e. a slow relaxation of the magnetization). In fact, these systems remain in a paramagnetic phase at any temperature.

More recently, one-dimensional (1-D) systems [14,15], termed Single-Chain Magnets (SCMs) [15,16], have been discovered to exhibit slow relaxation of the magnetization and thus magnet properties comparable to SMMs. While most of the previous reviews on SCMs are describing their chemistry and synthetic strategies to obtain this type of systems [17,18,19,20,21,22,23,24], this report is mainly focusing on the magnetic properties of Single-Chain Magnets and related systems. It summarizes the current knowledge on a theoretical point of view and illustrates the different aspects with selected experimental data. In SCM materials, the slow relaxation of the magnetization is not the signature of isolated anisotropic complexes like for SMMs, but arises from the magnetic interactions between anisotropic repeating units along a single chain. As a result, the SCM phenomenon is due to the critical slowing down observed at the neighborhood of a second order magnetic transition occurring at 0 K in the one-dimensional case. Hence, the presence of a short range order along the chain induces a slowing down of the spin dynamics over a broad range of temperatures. This dynamic was first by R. J. Glauber in 1963 in the frame of the Ising model [25]. Since the increase of the intrachain interaction is much easier to control experimentally than the intrinsic magnetic anisotropy in SMMs, SCMs are a promising alternative for information storage [15-24].

For the first time in 2002, a chain of ferromagnetically coupled units, as imagined by R. J. Glauber [25] ($[Mn_2(saltmen)_2Ni(pao)_2(py)_2](ClO_4)_2$; $saltmen^{2-}$: *N*,*N*'–(1,1,2,2-tetramethylethylene)-bis(salicylideneiminate); pao^-: pyridine-2-aldoximate; py: pyridine), was synthesized and its SCM properties studied in details [15]. In this system shown in Fig. 2, the choice of the precursor building-blocks ($[Mn_2(saltmen)_2(H_2O)_2](ClO_4)_2$ and $[Ni(pao)_2(py)_2]$) allowed a premeditated control of the structural dimensionality and opened the possibility to design a large series of one-dimensional systems of general formula: $[Mn_2(5\text{-}Rsaltmen)_2Ni(L1)_2(L2)_x](X)_2$ (noted in the following $[Mn_2Ni]$ chains; $Rsaltmen^{2-}$: *N*,*N*'–(1,1,2,2-tetramethylethylene)-bis(5-Rsalicylideneiminate); R: H or MeO; L1: pao^-: pyridine-2-aldoximate or $miao^-$: 1-methylimidazole-2-aldoximate or $eiao^-$: 1-ethylimidazole-2-aldoximate; L2: $x = 2$ for pyridine, 4-picoline, 4-*tert*-butylpyridine or *N*-methylimidazole, $x = 1$ for 1,10 phenanthroline; X^-: $[ClO_4]^-$, $[ReO_4]^-$, $[BPh_4]^-$, $[PF_6]^-$, $[BF_4]^-$) [15,26,27,28]. In this family of compounds, the strong antiferromagnetic coupling between Mn^{III} and Ni^{II} spin carriers leads at low temperatures (typically below 25 K) [15,26-28] to $S = 3$ macrospin units, which

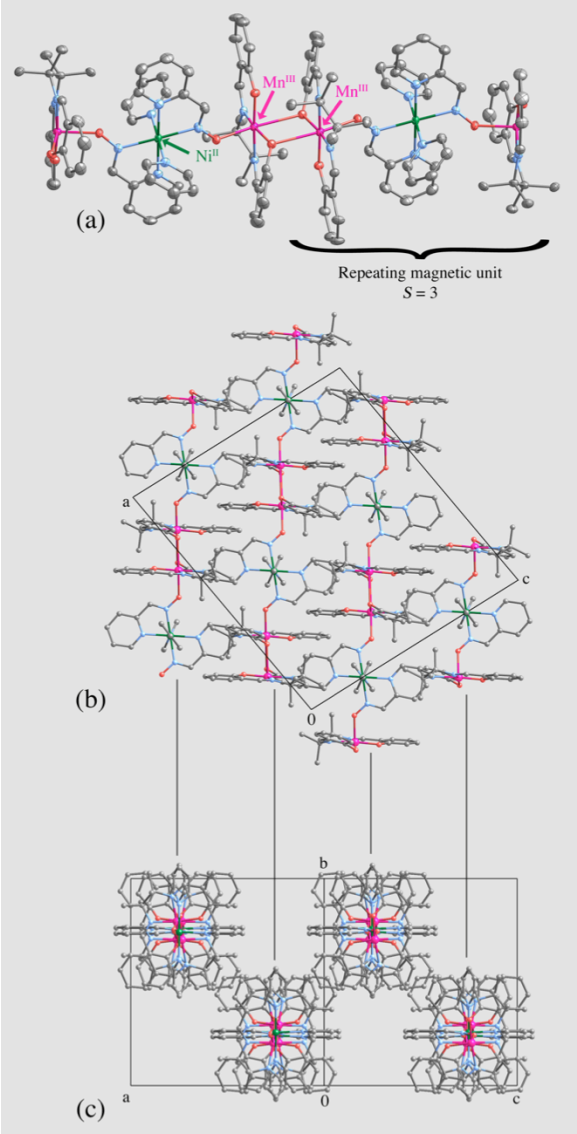

Figure 2. Views of the crystal structure of $[Mn_2(saltmen)_2Ni(pao)_2(py)_2](ClO_4)_2$; (a) the one-dimensional arrangement; (b) a projection in the (*ac*) plan, and (c) a projection along the chain axis. The hydrogen atoms and perchlorate anions located between the chains have been omitted for clarity. Color code: blue: N, red : O, pink: Mn, green: Ni, grey: C. Adapted from ref. 15.

are ferromagnetically coupled along the chain. Up to date, this system appears to be one of the simplest experimental illustration of a SCM made of ferromagnetically coupled anisotropic spins in the Ising limit (i.e. large anisotropy energy in

comparison to the intra-chain exchange energy). The first part of this book chapter (section 2) is summarizing the theoretical description of this type of SCMs and selected experimental data from the $[Mn_2(5\text{-Rsaltmen})_2Ni(L2)_2(L1)_x](X)_2$ compounds have been chosen to illustrate the key conclusions [15,26-28].

In section 3, the magnetic properties of regular chains of antiferromagnetically coupled anisotropic spins will be described and discussed in relation with the dual ferromagnetic case presented in section 2. Indeed, slow relaxation of the magnetization is also expected in this type of chain due to finite-size effects. Experimental data from the $[Mn_4(hmp)_6(L)_2](ClO_4)_2$ compounds (Hhmp: 2-hydroxymethylpyridine; L^-: N_3^-, CH_3COO^-, $ClCH_2COO^-$) made of antiferromagnetically coupled $S = 9$ anisotropic $[Mn_4(hmp)_6]^{4+}$ motifs [29,30], will be used to illustrate this part.

The fourth part of this chapter is devoted to the effect of the inter-chain interactions and the possibility to stabilize three-dimensional magnetic orders of chains that, individually, would behave as a SCM. In contradiction with what was usually believed, it has been recently demonstrated both theoretically and experimentally (for example in $[Mn_2(5\text{-MeOsaltmen})_2Ni(pao)_2(phen)](PF_6)_2$) [31] that slow relaxation of the magnetization, i.e. magnet type behavior induced by the presence of the chains, is still present in the magnetic ordered state, even in the case of an antiferromagnetic ground state [32,33].

Concluding remarks and perspectives will be finally given in Section 5. In particular, the case of single-chain magnets that display more complex structure or spin topologies will be evoked.

2
Regular chain of ferromagnetically coupled anisotropic spins

As mentioned in the introduction, numerous systems have been recently described as Single-Chain Magnets. However, many of them have been characterized only in a very preliminary manner and then it is not excluded that some of them may present a 3-D long range magnetic order and not SCM properties (see section 4). To fully characterize a SCM, detailed static (thermodynamic) and dynamic magnetic measurements are required. To illustrate this argument, we will take the example of the $[Mn_2Ni]$ chain [15,26-28], already mentioned in the introduction. In fact, this family of one-dimensional coordination polymers can be considered as a model system from which theoretical arguments and experimental results can be nicely compared. The dynamic properties and in particular the slow relaxation of the magnetization are essential. However, the static properties should be in priority and extensively described since they are at the origin of the magnetization dynamics of the chain.

2.1
Basic arguments

Fig. 2 shows different views of the crystal structure of the $[Mn_2(saltmen)_2Ni(pao)_2(py)_2](ClO_4)_2$ chain [15]. Thanks to the organic ligands, the different chains are well isolated from each others in the crystal structure and, therefore, they can be considered as magnetically isolated. However, the magnitude of the interchain interactions cannot be easily quantified by a simple examination of the structure and thus this hypothesis should be verified by a detailed analysis of the static magnetic properties of the material (*vide infra*). Considering a single chain, Fig. 2a shows that the complexes organization can be described either in terms of Mn-Ni-Mn trinuclear units or Mn-Mn dinuclear complexes linked by $[Ni(pao)_2(py)_2]$ modules. For the magnetic analysis, the first description is the most appropriate as the exchange interaction within the Mn-Ni-Mn moieties is known to be about 2 orders of magnitude stronger than the Mn-Mn exchange coupling [15]. Consequently, only the ground state of the Mn-Ni-Mn trinuclear unit should be populated at low temperature allowing its approximation to an effective $S = 3$ macrospin. The coupling between Mn metal ions, J, being ferromagnetic ($J > 0$), the system can be described using this approximation as regular chain of ferromagnetically coupled effective $S = 3$ spins (Fig. 3).

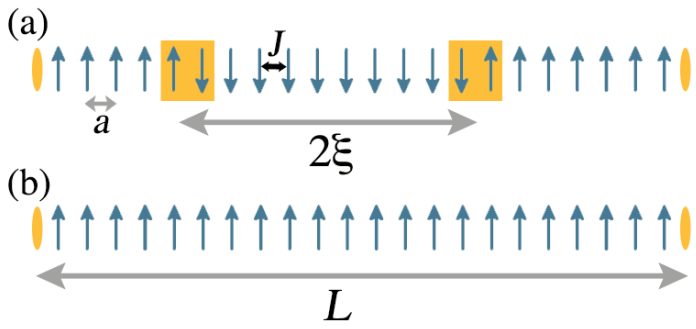

Figure 3. Schematic views of a chain of ferromagnetically coupled Ising-type spins in zero *dc* field in the case of $2\xi < L$ (a) and $2\xi >> L$ (b). L is the distance between two defects (orange ellipses). 2ξ is the size of the magnetic domains separated by two domain walls (orange squares) with ξ being the correlation length.

Due to the well-known Jahn-Teller distortion of the Mn^{III} coordination sphere, these effective spins should be described as anisotropic magnetic centers with a local easy axis oriented along the JT axis. In the crystal structure (Fig. 2), the magnetic easy axes are ideally oriented along a unique orientation coinciding with the chain direction. The relevant Hamiltonian (called anisotropic Heisenberg Hamiltonian) to describe this $[Mn_2Ni]$ chain in absence of an applied field, is given by Eq. 1, in which the S_i spins are considered as classical spins.

$$H = -2J\sum_{-\infty}^{+\infty}\vec{S}_i\vec{S}_{i+1} - D\sum_{-\infty}^{+\infty}S_{iz}^2 \quad (1)$$

With the convention adopted in this Hamiltonian, Eq. 1, $D > 0$ corresponds to an easy axis. In the simple limit where $D >> J$, the magnetic anisotropy forces the effective spin to align with the local easy axis and the above Hamiltonian is thus reduced to the Ising model (Eq. 2, where $\sigma_i = \pm 1$ specifies the orientation of the i^{th} spin).

$$H = -2JS^2\sum_i \sigma_i\sigma_{i+1} \quad (2)$$

In the next subsections, we will describe the static and dynamic properties of the regular chain of ferromagnetically coupled anisotropic spins (Fig. 3).

2.2 Infinite chain length regime

In this part, the simplest description of the chain will be presented in the absence of an applied magnetic field and considering a chain of infinite length (Fig. 3a; at this level of description, the unavoidable presence of defects is ignored).

2.2.1 Static properties

General considerations can be given for the anisotropic Heisenberg model. First, as for any 1-D system (with short range interactions), no long range magnetic order can be present at a finite temperature. However, a critical point does exist at $T = 0$ K and for this reason, short range order develops at low temperature. Independently of the D/J ratio, a general description of these one-dimensional spin systems with magnetic correlations can be done. In the low temperature limit, the equilibrium state of these chains consists of large oriented magnetic domains separated by narrower domain walls (Fig. 3a). As domains with positive or negative magnetization are equally probable in absence of an applied magnetic field, the average net magnetization of a chain is zero. The size of these domains is by definition equal to 2ξ, where ξ is the correlation length. In the low temperature limit, the temperature dependence of the correlation length can be easily deduced from a simple argument: the domain walls are well isolated from each other and therefore, they follow a Boltzmann statistics. Their number decreases exponentially as

exp(—E/k_BT) where E is the creation energy of a domain wall [16]. Consequently, the correlation length also increases exponentially as exp(E/k_BT) when the temperature is lowered. The profile of a domain wall has been calculated for regular chain of ferromagnetically coupled classical spins (at $T = 0$ K) [34]. This work has been recently revisited to include more complex configurations of the chain [35]. Fig. 4 gives the equilibrium profile for the regular ferromagnetic chain with different D/J ratios. While "broad" domain walls are found for small D/J values (Fig. 4a), a discontinuity appears in the center of the domain wall for intermediate values (Fig. 4b). Finally, as soon as $D/J > 4/3$ (Fig. 4c), the domain wall is remarkably identical to the one predicted for the Ising limit and implies only two spins of opposite orientations (Fig. 3). This crossover is also emphasized when plotting the equilibrium angle, θ_0, of the first spin situated on the right part of the domain wall ($n = 0$). Fig. 5a gives the evolution of this angle as a function of D/J.

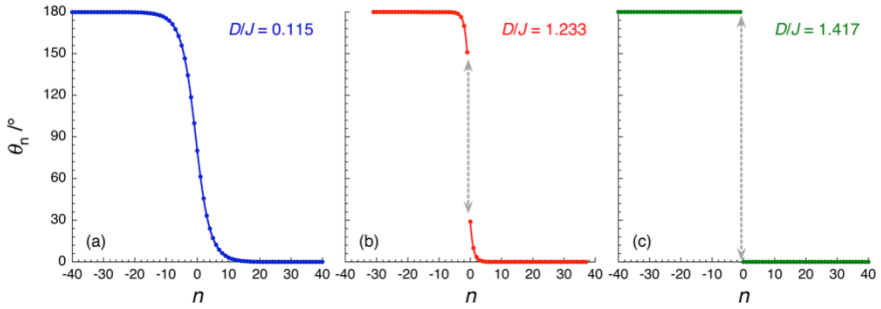

Figure 4. Angular equilibrium profile of the spin orientation (n is the index of a given spin along the chain) on both sides of a domain wall (as in reference 34, n = -1/2 corresponds the center of the domain wall) in (a) the broad domain wall limit, for (b) an intermediate value of D/J and in (c) the Ising limit with $D/J > 4/3$.

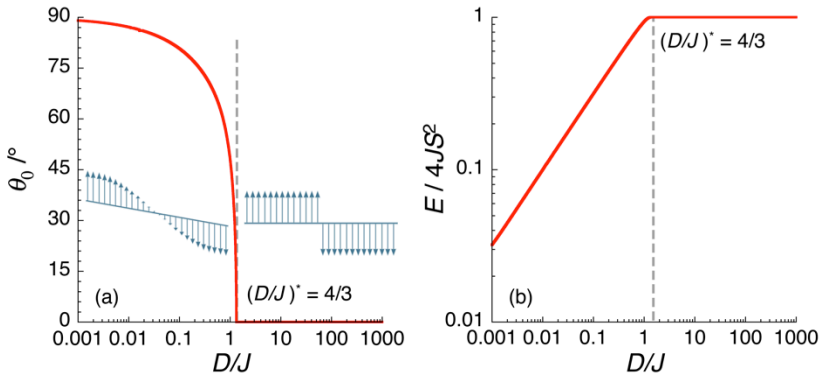

Figure 5. (a) Variation of the equilibrium angle of the $n = 0$ spin and (b) the corresponding energy E of the domain wall (normalized to $4JS^2$) as a function of D/J.

The corresponding creation energy of the domain wall is given in Fig. 5b. Although first increasing with D/J, this energy becomes constant and equal to $4JS^2$ as soon as D/J is larger than 4/3. The crossover between these two regimes, also evidenced by Fig. 5a, has been described at zero temperature as a phase transition [36]. The energy of the domain wall, E, can be probed experimentally measuring the parallel magnetic susceptibility ($\chi_{//}$) in the zero *dc*-field limit, that is proportional to the correlation length as shown in Eq. 3 (C is the Curie constant and a is the unit cell parameter along the chain; Fig. 3) [16,37]. Experimentally as illustrated by Fig. 6, the semi-log plot of χT versus $1/T$ at low temperature gives a thermally activated behavior with an energy gap usually called Δ_ξ (Eq. 3).

$$\frac{\chi_{//}T}{C} = \frac{2\xi}{a} = \exp\left(\Delta_\xi / k_B T\right) \tag{3}$$

In the Ising limit ($D >> J$), this experimental activation energy, Δ_ξ, is directly equal to the energy of the domain wall, $E = 4JS^2$. In the case of a finite anisotropy, Δ_ξ is still equal to E (Fig. 5b), at enough low temperature, as proved analytically by Nakamura et al [38,39]. However, other magnetic excitations, like spins waves, may be relevant at higher temperatures and the activation energy of the relaxation time may be affected [40]. This latter point has been recently discussed based on numerical calculations by Vindigni et al [41].

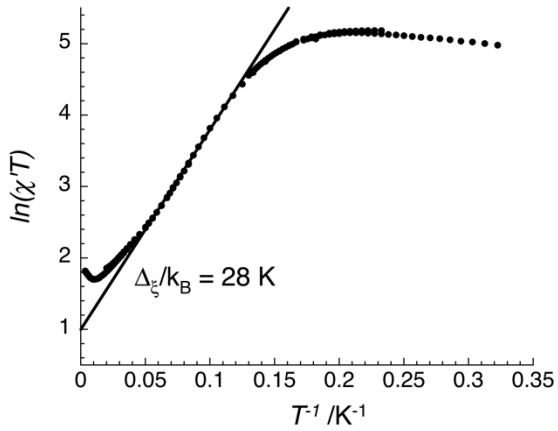

Figure 6. Plot of $\ln(\chi'T)$ versus $1/T$ for $[Mn_2(saltmen)_2Ni(pao)_2(py)_2](ClO_4)_2$ (χ' is the in-phase component of the ac susceptibility measured in zero *dc* field at 1 Hz). Adapted from ref. 42.

Fig. 6 gives an example of this kind of experimental results for the $[Mn_2Ni]$ chain [42]. Between 7.5 K and 25 K, a linear dependence is clearly observed with Δ_ξ/k_B = 28 K. Above 25 K, the effective spin approximation fails and the $\ln(\chi T)$ value

deviates from a straight line. Below 7.5 K, a saturation of the χT product is observed due to the finite size effects, as discussed in the section 2.3. The deduced Δ_ξ value is consistent with the estimation of $4JS^2$, indeed expected for these [Mn_2Ni] chain systems, which fall in the Ising limit i.e. $D/J > 4/3$. In the rest of this section, including the dynamic properties, the discussion will be developed within the Ising limit.

Note that the data shown in Fig. 6 are obtained on a polycrystalline sample. Hence, the measured magnetic susceptibility, χ, should contain both parallel (to the easy magnetic axis, Eq. 3) and perpendicular contributions as shown in Eq. 4.

$$\chi = \frac{2\chi_\perp + \chi_{//}}{3} = \frac{2}{3}\chi_\perp + \frac{C}{3T}\exp\left(4JS^2/k_BT\right) \tag{4}$$

However, the transverse contribution is negligible at low temperature as the parallel component becomes large. The thermally activated behavior is thus readily observed on a polycrystalline sample without any significant correction due to the transverse susceptibility.

2.2.2 Dynamic properties

The application of a *dc* field on a SCM system generates a finite magnetization. When this applied field is suppressed, the induced magnetization decreases with time to finally relax to zero as expected at the thermal equilibrium. In order to understand these relaxation properties, it is thus necessary to describe the time dependence of the magnetization. Alternatively, the dynamics of the magnetization can be studied when probing the magnetic response with a small alternative (*ac*) field applied at a given frequency, ν. As the frequency dependence of the *ac* susceptibility is the Fourier transform of the time response, this *ac* technique gives the same information as the time resolved *dc* measurement. Indeed, most of the experimental studies reported on SCMs have been performed with *ac* susceptibility measurements on polycrystalline samples.

In the simplest case, the magnetic relaxation corresponds to the existence of a single mode, i.e. to a Debye model [43]. In this approximation, the real and imaginary part of the *ac* complex susceptibility are given by Eq. 5 (where χ_{dc} is the static magnetic susceptibility and $\omega = 2\pi\nu$).

$$\chi'(\omega) = \frac{\chi_{dc}}{1+\omega^2\tau^2} \quad \text{and} \quad \chi''(\omega) = \frac{\chi_{dc}\omega\tau}{1+\omega^2\tau^2} \tag{5}$$

The position of the $\chi''(\omega)$ maximum readily gives the relaxation time at a given temperature as $\omega_{max}\tau = 1$ with $\omega_{max} = 2\pi\nu_{max}$ (ν_{max} is the frequency at which the maximum of χ'' is observed). Fig. 7 gives selected *ac* data measured for the [Mn_2Ni] chain [44]. As a first approximation, the $\chi''(\nu)$ curves follow a generalized Debye model. In this case, the expressions given above (Eq. 5) are generalized introducing a third parameter, α, that takes into account a distribution of relaxation times [43]. This parameter being small, the assumption of a single relaxation time remains reasonable. The frequency position of the $\chi''(\nu)$ maximum and therefore the relaxation time, τ, are both temperature dependent and thus these measurements (Fig. 7) can be used to estimate the temperature dependence of τ.

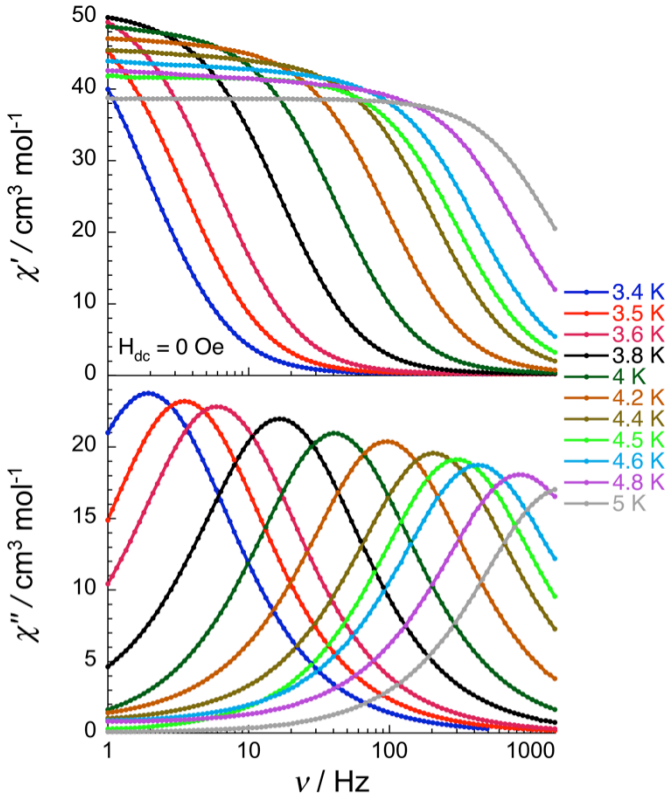

Figure 7. Frequency dependence between 1 and 1500 Hz of the in-phase and out-of-phase ac susceptibility between 3.4 and 5 K for $[Mn_2(saltmen)_2Ni(pao)_2(py)_2](ClO_4)_2$ [44].

It should be noted that in most publications, the temperature dependence of χ' and χ'' at a given frequency is reported. In order to determine the temperature dependence of the relaxation time, the maximum of $\chi''(T)$ at a given frequency is identified as the blocking temperature T_B. The deduced T_B versus ν plot is then reversed

to obtain τ versus $1/T_B$. This measurement strategy is neither logic nor without danger. Considering that both χ_{dc} and τ are temperature dependent, the maximum of $\chi''(T)$ (Eq. 6) does not give the right answer unless the temperature dependence of χ_{dc} is much weaker than the one of τ [45]. The determination of $\tau(T)$ by this method becomes completely wrong if several relaxation modes are present.

$$\chi''(T) = \frac{\chi_{dc}(T)\tau(T)\omega}{1+\omega^2\tau(T)^2} \tag{6}$$

For a theoretical description of the relaxation, the simplest approach relies on stochastic models, which have essentially been developed for Ising systems. Following the pioneering work of Glauber [25], most of the theoretical works assume the occurrence of single-spin flips during the relaxation process. In this case, the dynamics is described by elementary steps where the transition probability, $W_i(\sigma_i)$, to flip the i^{th} spin from σ_i to $-\sigma_i$ depends on the local field, E_i, seen by this spin. This local field is assumed to depend only on the spin state of the σ_i first neighbors. In the one dimensional Ising case (Eq. 2), E_i is given by Eq. 7.

$$E_i = 2JS^2(\sigma_{i-1} + \sigma_{i+1}) \tag{7}$$

Indeed, several choices for $W_i(\sigma_i)$ can be made with the only condition being that the detailed balance relation should be verified, to be consistent with the equilibrium probabilities shown in Eq. 8.

$$\frac{W_i(\sigma_i)}{W_i(-\sigma_i)} = \frac{\exp(-E_i\sigma_i/k_BT)}{\exp(E_i\sigma_i/k_BT)} = \frac{1-\sigma_i\tanh(E_i/k_BT)}{1+\sigma_i\tanh(E_i/k_BT)} \tag{8}$$

Where the right part equality of Eq. 8 is obtained only when $\sigma_i = \pm 1$. For the same reason, the most general way to express the transition probability is given in Eq. 9 with f being an even function of the local field [35].

$$W_i(\sigma_i) = f(E_i/k_BT)\left(1-\sigma_i\tanh(E_i/k_BT)\right) \tag{9}$$

The simplest choice for $W_i(\sigma_i)$ was suggested by Glauber [25] and corresponds to $f = 1/2\tau_0$, where τ_0 is the spin flip time for a spin in absence of interactions. In this case, Eq. 10 (with $\gamma = \tanh(4JS^2/k_BT)$ [25]) gives an equivalent expression of the transition probability (as $\sigma_i = \pm 1$).

$$W_i(\sigma_i) = \frac{1}{2\tau_0}\left(1 - \frac{\gamma}{2}\sigma_i(\sigma_{i-1} + \sigma_{i+1})\right) \tag{10}$$

Nevertheless, the choice of the transition probability made by Glauber is arbitrary with the only motivation to be able to find an exact mathematical solution of this equation system in absence of an applied *dc* field. In fact, a more physical probability law would be an Arrhenius law [46,47,48]. In this case the transition probability is given by Eq. 11 for $f(E_i/k_BT) = \cosh(E_i/k_BT)/(2\tau_0)$.

$$W_i(\sigma_i) = \frac{1}{2\tau_0}\exp\left(-E_i\sigma_i / k_BT\right) \tag{11}$$

In the one-dimensional case, a general expression of $W_i(\sigma_i)$ can be established (Eq. 12) independently of the transition probability choice.

$$W_i(\sigma_i) = \frac{1}{2\tau_0(1-\rho)}\left(1 + \rho\sigma_{i-1}\sigma_{i+1} - \frac{\gamma}{2}(1+\rho)\sigma_i(\sigma_{i-1} + \sigma_{i+1})\right) \tag{12}$$

In Eq. 12, ρ is a function of the temperature, which depends on the probability law. While $\rho = 0$ in the special case of the Glauber probability, ρ is equal to $\tanh^2(2JS^2/k_BT)$ in the Arrhenius case [35]. Independently of ρ, the next step to calculate the relaxation time is the determination of dynamic equations (Eq. 13) for the average correlation functions.

$$\frac{d<\sigma_i\sigma_j...\sigma_r>}{dt} = -2<\sigma_i\sigma_j...\sigma_r\left(W_i(\sigma_i) + W_j(\sigma_j) + ... + W_r(\sigma_r)\right)> \tag{13}$$

Eq. 13 contains indeed a large number of coupled differential equations, with the first of these equations given by Eq. 14.

$$\tau_0(1-\rho)\frac{d<\sigma_i>}{dt} + \left(1 - \gamma(1+\rho)\right)<\sigma_i> + \rho<\sigma_{i-1}\sigma_i\sigma_{i+1}> = 0 \tag{14}$$

When $\rho = 0$ (Glauber probability), Eq. 14 describes the dynamics of the magnetization decoupled from the rest of the equation system. Only in this particular case, this dynamic equation is exactly solvable leading to an exponential time decay of the magnetization with a single relaxation time given by Eq. 15. In the low temperature limit, Eq. 15 can be simplified and τ is then given by Eq. 16.

$$\tau = \frac{\tau_0}{1 - \tanh\left(4JS^2/k_BT\right)} \tag{15}$$

$$\tau = \frac{\tau_0}{2}\exp\left(8JS^2/k_BT\right) \tag{16}$$

On the other hand, no obvious analytical solution can be found even in the Arrhenius case, even in zero *dc* field, as the dynamics of the magnetization is coupled to the one of a three spins correlation function that is itself coupled to higher order terms! To discuss the effect of the probability law, numerical calculations are then necessary. Recent results include solutions from (i) the diagonalization of the whole dynamic linear equations system (Eq. 13) on small chains (up to 10 spins) and (ii) Monte Carlo simulations on larger systems of N spins [35] with different boundary conditions: either finite rings or open chains. Fig. 8 shows typical magnetization relaxations calculated in the Arrhenius case for $N = 100$ (note that these results are representative of any chain length). Single exponential relaxations are found with both boundary conditions. No significant difference in Fig. 8a can be found between open chains and finite rings when the correlation length, 2ξ, is smaller than the chain length, $L = aN$ (Fig. 3), while different relaxation times are clearly observed for $2\xi > L$ (Fig. 8b). This latter point highlights the presence of finite size effects that will be discussed in the next section (2.3).

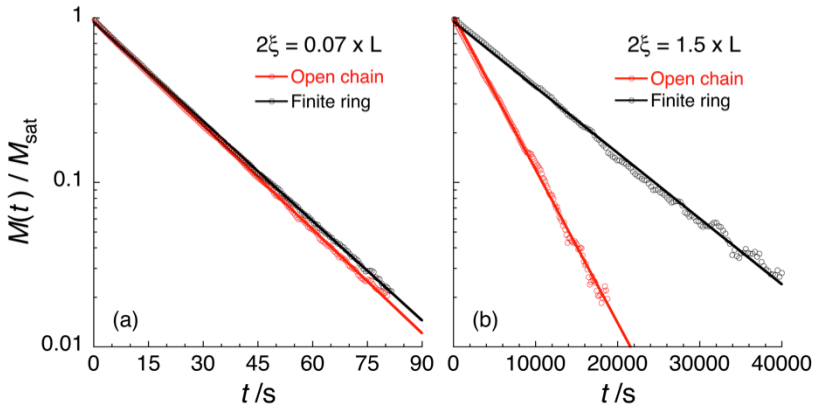

Figure 8. Time decay of the normalized magnetization considering the Arrhenius probability law simulated by Monte Carlo approach (for $N = 100$) showing the single exponential behavior, when (a) $2\xi < L$ and (b) $2\xi > L$ (i.e. at lower temperature). Solid line are the best fit of the numerical results by exponential laws.

As single exponential relaxations of the magnetization are obtained (Fig. 8), a single relaxation time is readily deduced from these numerical data. It is important to note that τ is normalized by τ_0 in Fig. 9 and thus only the contribution due to the magnetic correlations is shown. It is absolutely remarkable to observe in Fig. 9 that the obtained relaxation time and its temperature dependence are essentially the same for the Glauber and Arrhenius probability laws. In contrast with what was claimed in previous publications on the subject, these simulations demonstrate that the slow relaxation of the magnetization in SCM systems is not necessary a Glauber dynamics! As it will be discussed in section 2.4, it is indeed not possible to discriminate between the probability laws with experimental results at zero *dc* field.

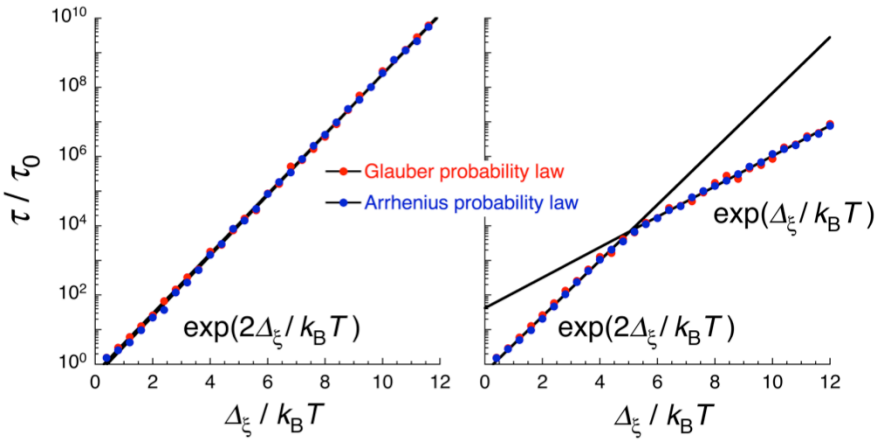

Figure 9. Deduced normalized relaxation time (for $N = 100$; from Fig. 8) as a function of the inverse of the normalized temperature for (a) finite ring and (b) open chain. The black solid lines are indicating the exponential laws for the different regimes of relaxation.

For the finite ring, the relaxation time is following a single thermally activated law in agreement with Eq. 16 (Fig. 9a). In contrast, as seen in Fig. 9b, a crossover is observed for open chains. At high temperature, the relaxation time follows the same exponential law as for the finite ring, while the activated energy is reduced by two below the crossover temperature, T^*. This crossover, also related to the presence of finite size effects, will be discussed in the section 2.3.

These simulations show clearly that the relaxation of the magnetization exhibits a universal behavior at zero field and low temperatures that is independent of the chosen probability law. Indeed this result can be inferred from simple scaling arguments (omitting numerical factors). The relaxation time is the characteristic time for a domain wall to diffuse on the length ξ of a magnetic domain. The elementary time unit being τ_0, one gets immediately $\tau \propto \tau_0(\xi/a)^2$ [49]. Therefore considering Eq. 3, the relaxation time in the Ising limit is thermally activated with an energy gap of $2\Delta_\xi$ (Eq. 17).

$$\tau = \frac{\tau_0}{2}\exp\left(2\Delta_\xi / k_B T\right) \tag{17}$$

The observed universality is also consistent with the vicinity of a critical point for $T = 0$ in absence of magnetic field for which the dynamic behavior is no longer dependent on the details of the model, like the expression of the probability law. This important, although often ignored, argument has a straightforward consequence: the experimental data obtained only at zero *dc* field cannot be used to claim that the Glauber model has been verified. Only the above scaling arguments, valid for a whole class of probability laws, are probed with such experiments.

Finally, to compare with experimental data, it should be mentioned that τ_0 is also expected to follow an activated law (Eq. 18) with an energy gap, Δ_A, that is the energy barrier experienced by a spin unit in absence of interaction, i.e. inside a domain wall.

$$\tau_0(T) = \tau_i \exp\left(\Delta_A / k_B T\right) \tag{18}$$

In the Ising limit (for narrow domain walls), Δ_A is equal to DS^2. Finally from Eq. 17 and 18, the relaxation time for the infinite chain at low temperature can be deduced as shown by Eq. 19 (the pre-factor τ_i describes the intrinsic dynamics of the spin in contact with the thermal bath, in the absence of an energy barrier).

$$\tau = \frac{\tau_i}{2}\exp\left(\left(2\Delta_\xi + \Delta_A\right)/k_B T\right) \tag{19}$$

This relation is expected to be also true for a finite anisotropy, at least in the low temperature limit. Of course in this case, the expressions of Δ_ξ and Δ_A may be more complicated that the one found in the Ising limit (where $\Delta_\xi = 4JS^2$ and $\Delta_A = DS^2$). For example, the expression of Δ_A in the large domain wall limit ($D << J$) is still controversial [41].

The temperature dependence of the experimental relaxation time for the $[Mn_2Ni]$ chain is given in Fig. 10. As expected theoretically (*vide supra*), two thermally activated regimes are observed with $\Delta_{\tau 1}/k_B = 74$ K and $\Delta_{\tau 2}/k_B = 55$ K respectively. As DS^2 can be determined, for example, from M versus H data on an oriented single crystal when the magnetic field is applied along the hard axis, the above relation (Eq. 19) can be tested experimentally. In the case of the $[Mn_2Ni]$ chain (Fig. 10), the equality $\Delta_{\tau 1} = 2\Delta_\xi + \Delta_A$ is experimentally verified with $\Delta_\xi/k_B = 28$ K and $\Delta_A/k_B = 23$ K. The low temperature regime where $\Delta_{\tau 2} = \Delta_\xi + \Delta_A$ will be discussed in the next section.

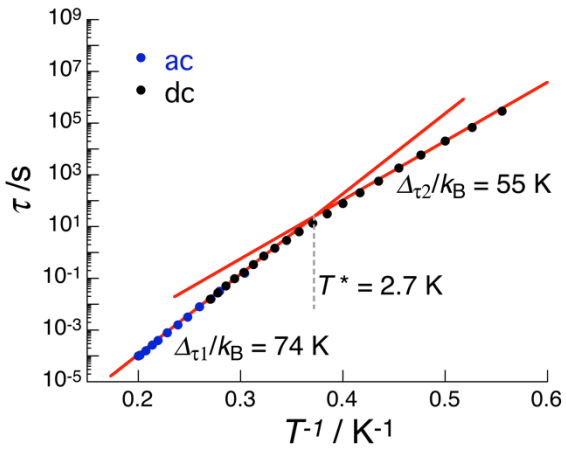

Figure 10. Semilog plot of the relaxation time τ versus $1/T$ for $[Mn_2(saltmen)_2Ni(pao)_2(py)_2](ClO_4)_2$. The blue and black dots were obtained from ac and dc measurements, respectively. The red straight lines are the Arrhenius laws in the infinite and finite-size chain regimes. Adapted from Ref. 42.

2.3 Finite size effects

As noticed in the previous section for the $[Mn_2Ni]$ chain, the experimental results (Fig. 6 and 10) deviate significantly from the expected infinite chain behavior at low temperatures. This feature, that is quite general in SCM systems, reveals the presence of defects along the spin chain. Defining L as the average distance between two defects (Fig. 3b), it is clear that the magnetic correlations along the chain should saturate below the temperature for which $L \approx 2\xi$ (where ξ is the theoretical correlation length of the chain without defects) inducing, for $2\xi >> L$, the presence of only one magnetic domain between two defects. This crossover generated by finite size effects can be predicted by Monte Carlo simulations (Fig. 8b and 9b) as well as observed experimentally (Fig. 6 and 10). Therefore, both static and dynamic properties of SCM systems will be revisited in the following paragraphs when $L > 2\xi$.

2.3.1 Static properties

The simplest approach to describe the finite size effects in SCMs is to consider the "monodisperse description". At this approximation, the chains are identical finite

segments of size L, i.e. the distance L between two defects is assumed to be a constant. Below the crossover temperature, T^*, when $\xi >> L$, the magnetic susceptibility is given by Eq. 20.

$$\frac{\chi T}{C} = \frac{L}{a} \tag{20}$$

In this limit, as there is only one magnetic domain per segment of size L, it can be considered as an effective LS/a spin. Thus, the above expression (Eq. 20) is simply the Curie law for these effective spins. Therefore, a saturation of the χT product is expected in presence of finite size effects as observed experimentally for the [Mn_2Ni] chain below 7.5 K (Fig. 6) [42]. In this case, the weak decrease of χT observed at low temperature has been attributed to small antiferromagnetic interactions between segments [42].

A polydisperse approach can also be developed [50,51] considering the probability c of finding a defect in the chain. Then, the probability of finding a chain of n spins is proportional to $c^2(1\text{-}c)^n$ for missing sites and $c^2(1\text{-}c)^{n\text{-}1}$ for missing links or interactions. In this case, the magnetic susceptibility can be calculated in the Ising limit for a chain of ferromagnetically coupled spins (S). Eq. 21 gives the analytical expressions of the χT product with $\eta = 1$ for missing links and $\eta = 1 - c$ for missing sites.

$$\frac{\chi T}{C} = \eta \frac{1+(1-c)\tanh\left(2JS^2/k_BT\right)}{1-(1-c)\tanh\left(2JS^2/k_BT\right)} \tag{21}$$

At the low temperature limit ($2JS^2 >> k_BT$) and when c is small (i.e. small number of defects), Eq. 21 can be simplified to a unique expression given by Eq. 22.

$$\frac{\chi T}{C} = \frac{2}{c+2\exp\left(-4JS^2/k_BT\right)} \tag{22}$$

The polydisperse approach also predicts a saturation of the χT product at low temperature at a value giving the average number of sites between two defects. It is worth mentioning that the temperature dependences of the magnetic susceptibility deduced from the monodisperse and polydisperse models are very similar and thus static measurements cannot help to detect the presence of polydispersity for a chain with ferromagnetically coupled spins [16].

2.3.2
Dynamic properties

Finite size effects on the relaxation time of one-dimensional systems have also been discussed using a monodisperse model and the Glauber probability law [52]. In this case, the relaxation time of the magnetization is governed by the longest characteristic time of a segment of size L. As previously discussed, τ experiences a crossover when $L \approx 2\xi$ (Fig. 9b and 10). Below this crossover, when $L << \xi$, the expression of the relaxation time is given in the Ising limit by Eq. 23 or in the general case by Eq. 24. Introducing the expression of τ_0 (Eq. 18), Eq. 24 can be simplified to Eq. 25.

$$\tau = \frac{\tau_0 L}{2a} \exp\left(4JS^2 / k_B T\right) \tag{23}$$

$$\tau = \frac{\tau_0 L}{2a} \exp\left(\Delta_\xi / k_B T\right) \tag{24}$$

$$\tau = \frac{\tau_i L}{2a} \exp\left(\left(\Delta_\xi + \Delta_A\right) / k_B T\right) \tag{25}$$

This theoretical result can be readily compared with the low temperature properties of the [Mn_2Ni] chain shown in Fig. 10. The experimental activation energy, $\Delta_{\tau 2}/k_B$ = 55 K, is in fact close to the expected $\Delta_\xi + \Delta_A$ sum, with Δ_ξ/k_B = 28 K and Δ_A/k_B = 23 K [42].

Dynamic properties have also been discussed in the frame of the polydisperse approach. In contrast with the monodisperse case, the theory predicts a non-exponential relaxation of the magnetization but the temperature dependence of the characteristic relaxation time is still given by the equations obtained from the monodisperse approach (Eq. 23-25) [53]. For this reason, the experimental results in the finite size regime are generally analyzed using the monodisperse approach.

Finally, it should be noted that the above conclusions are again independent of the probability law as shown by Fig. 9b, which compares the Glauber and Arrhenius results for a finite chain of 100 spin units.

2.4 Effect of the applied magnetic field

Only a very few experiments on SCMs have been performed in the presence of an applied magnetic field. However, the obtained data are essential to prove the SCM properties and to exclude the occurrence of a 3-D magnetic order. It is important to keep in mind that the slow relaxation of the magnetization in 1-D systems is due to the presence of a critical point located at $T_C = 0$ K and $H_C = 0$. Therefore, important variations of the static and dynamic properties should occur, not only by changing the temperature for $H = 0$, but also by increasing the applied magnetic field at a constant low temperature. In this latter case, a maximum of the magnetic susceptibility and of the relaxation time should be observed at $H = 0$ and an associated critical behavior should be present at low field. For the Ising model, the nature of this critical behavior has been extensively discussed, in particular to analyze the helix-coil transition in biopolymers [54,55,56,57,58,59,60,61]. The effect of an applied *dc* field on the SCM properties has been also described in a recent publication [62] and analyzed from numerical calculations [35]. The main results will be summarized in the next paragraphs.

2.4.1 Static properties

The field dependence of the magnetization can be exactly determined for an infinite chain of spins. In the Ising limit, the normalized magnetization, M/M_{sat} and the associated magnetic susceptibility, χ, are given by Eq. 26 and 27 respectively, with $M_{sat} = N\mu$ being the magnetization at saturation for N spins possessing an individual magnetic moment $\mu = g\mu_B S$.

$$\frac{M}{M_{sat}} = \frac{\sinh\left(\mu H / k_B T\right)}{\sqrt{\sinh^2\left(\mu H / k_B T\right) + \exp\left(-8JS^2 / k_B T\right)}} \tag{26}$$

$$\chi = \frac{\partial M}{\partial H} = \frac{M_{sat}\mu}{k_B T} \frac{\cosh\left(\mu H / k_B T\right)\exp\left(-8JS^2 / k_B T\right)}{\left(\sinh^2\left(\mu H / k_B T\right) + \exp\left(-8JS^2 / k_B T\right)\right)^{3/2}} \tag{27}$$

This expression of the magnetic susceptibility emphasizes the existence of a critical regime at low field ($\mu H << k_B T$) for which Eq. 27 simplifies into Eq. 28.

$$\chi = \frac{N\mu^2}{k_B T} \frac{\exp\left(4JS^2/k_B T\right)}{\left(1+\left(\mu H/k_B T\right)^2 \exp\left(8JS^2/k_B T\right)\right)^{3/2}}$$
$$= \frac{\chi(H=0)}{\left(1+\left(\mu H/k_B T\right)^2 \exp\left(8JS^2/k_B T\right)\right)^{3/2}} \quad (28)$$
$$= \frac{\chi(H=0)}{\left(1+(x)^2\right)^{3/2}}$$

Eq. 28 shows the existence of a reduced variable $x = (\mu H/k_B T) \exp(4JS^2/k_B T) = 2\mu H\xi/(ak_B T)$ that controls the field dependence of the magnetic susceptibility. At low temperature and as expected, the susceptibility is maximum at $H = 0$ (and $x = 0$) and is drastically reduced even at low fields (for $x \approx 1$).

For a spin segment of size L, finite size effects are predicted by the theory. In the simple limit where $\xi >> L$, all the spins are parallel within the segments. Each segment is then equivalent to a giant spin $nS = LS/a$. As an assembly of monodispersed segments follows a Boltzmann statistics, its magnetization and magnetic susceptibility can be easily expressed by Eq. 29 and 30 with a new reduced variable x' equal to $L\mu H/(ak_B T)$ (with the segment length, L, replacing 2ξ). In the low field limit ($x' << 1$), Eq. 30 can be simplified into Eq. 31. A critical effect is still observed with a maximum of the susceptibility at $H = 0$ ($x' = 0$) and its reduction at low fields (for $x' > 0$).

$$\frac{M}{M_{sat}} = \tanh\left(L\mu H/(ak_B T)\right) \quad (29)$$

$$\chi = \frac{L\mu}{ak_B T}\left(1 - \tanh^2\left(L\mu H/(ak_B T)\right)\right) \quad (30)$$

$$\chi = \frac{L\mu}{ak_B T}\left(1 - x'^2\right) \quad (31)$$

2.4.2
Dynamic properties

To discuss the effect of an applied magnetic field on the dynamic of SCMs, the transition probability should be generalized under *dc* field. In its pioneer work [25], Glauber reported a new expression of the transition probability given by Eq. 32 with $Q = \tanh(\mu H/k_B T)$.

$$W_i(\sigma_i) = \frac{1}{2\tau_0}(1 - Q\sigma_i)\left(1 - \frac{\gamma}{2}\sigma_i(\sigma_{i-1} + \sigma_{i+1})\right) \tag{32}$$

It should be mentioned that Eq. 32 was used by Glauber to describe only small applied fields. For higher fields, the above expression is no longer a simple function of the local field. For this reason, an alternative expression, Eq. 33, was introduced by Suzuki and Kubo [63] (with E_i defined by Eq. 7). It is worth noting that Eq. 33 becomes identical to the Glauber expression in zero field (Eq. 32).

$$W_i(\sigma_i) = \frac{1}{2\tau_0}\left(1 - \sigma_i \tanh\left(\frac{E_i + \mu H}{k_B T}\right)\right) \tag{33}$$

Finally in the Arrhenius case, the transition probability can also be written in presence of an applied field as shown by Eq. 34 [47,48].

$$W_i(\sigma_i) = \frac{1}{2\tau_0}\exp\left(-\frac{2JS^2}{k_B T}\sigma_i(\sigma_{i-1} + \sigma_{i+1}) - \frac{\mu H}{k_B T}\sigma_i\right) \tag{34}$$

In each case, the relaxation of the magnetization can be calculated solving a system of coupled dynamic equations, exemplified by Eq. 35 for the Glauber transition probability.

$$\tau_0 \frac{d<\sigma_i>}{dt} + (1-\gamma)<\sigma_i> + \gamma Q <\sigma_i \sigma_{i+1}> - Q = 0 \tag{35}$$

Even in this simple case, this equation is not decoupled from the rest of the system and thus an exact solution is no longer available. Unfortunately, this remark is also true for the Suzuki-Kubo and Arrhenius probability laws. Although the Glauber model is no longer exactly soluble for $H \neq 0$, simple approximations like the local equilibrium approximation (LEA) have been used to obtain a solution [62]. The spirit of this approximation is to consider first the linear response of the system.

The linearized version of Eq. 35 is given by Eq. 36 introducing $m = <\sigma_i>$, $\Gamma = <\sigma_i \sigma_{i+1}>$ and $\delta m = m(t) - m_{eq}$ (m_{eq} being the equilibrium value of m). The relaxation time is thus easy expressed as a function of γ, Q and dΓ/dm in Eq. 37.

$$\tau_0 \frac{d\delta m}{dt} + \left(1 - \gamma + \gamma Q \frac{d\Gamma}{dm}\right)\delta m = 0 \tag{36}$$

$$\frac{\tau_0}{\tau} = 1 - \gamma + \gamma Q \frac{d\Gamma}{dm} \tag{37}$$

The LEA consists in introducing the equilibrium value of dΓ/dm in Eq. 37, considering that the relaxation of the correlation function Γ is much quicker than the relaxation of the magnetization.
As for the static properties, a critical regime is found at low fields. For the infinite chain, the deduced relaxation time is given by Eq. 38.

$$\tau(H) = \frac{\tau(H=0)}{1 + \left(\mu H / k_B T\right)^2 \exp\left(8JS^2 / k_B T\right)} = \frac{\tau(H=0)}{1 + x^2} \tag{38}$$

Therefore, as concluded for the magnetic susceptibility, the relaxation time of the magnetization for a SCM is expected to be maximum at $H = 0$ ($x = 0$) and to decrease rapidly when a magnetic field is applied. This conclusion holds also in the finite size regime for which the relaxation is given by Eq. 39 at low fields.

$$\tau(H) = \frac{\tau(H=0)}{1 + 2\left(\mu H / k_B T\right)^2 L^2 / 3a^2} = \frac{\tau(H=0)}{1 + 2x'^2/3} \tag{39}$$

Omitting the numerical factors, the two expressions are similar and emphasize the role of x or x' as reduced variables to describe the critical effects.
To avoid these approximations, numerical results have been recently obtained [35]. Although they confirm qualitatively the scaling laws deduced from the LEA, they show that the field dependence found in Eq. 38 and 39 is overestimated by a factor 2. The origin of this discrepancy is found in the calculation of dΓ/dm that appears in Eq. 37.[1] Then, Eq. 38 and 39 for the Glauber case must be replaced by

[1] The equilibrium value of Γ is an even function of m and Γ is proportional to m^2 or Hm at low field. The estimation of d(Hm) at the LEA gives Hdm + mdH = 2 Hdm (as m is proportional to H at equilibrium and low field). On the other hand, the dynamic calculation requires the estimation of d(Hm) for a constant value of H, which is exactly half of the LEA result.

the corrected expressions, Eq. 40 and 41, for the infinite and finite size regimes, respectively.

$$\tau(H) = \frac{\tau(H=0)}{1 + x^2 / 2} \tag{40}$$

$$\tau(H) = \frac{\tau(H=0)}{1 + x'^2 / 3} \tag{41}$$

Indeed, the field dependence of the relaxation time is not strongly modified by the choice of the probability law as expected in a critical regime, i.e. when x or x' << 1, for which a universal behavior must be observed. Outside the critical regime, the expressions of the relaxation time can also be established. Relying on the local equilibrium approximation, theoretical results have been obtained in the Glauber case. The main conclusion of this work demonstrates that τ becomes of the order of τ_0 for $x >> 1$ or $x' >> 1$ [62]. More recently, Monte Carlo simulations have been used to study the effect of the different probability laws on the magnetization relaxation under *dc* field [35]. Typical numerical data of the magnetization relaxation in the finite-size regime ($2\xi > L$) are shown in Fig. 11 starting from an initial state being completely saturated with a negative magnetization.

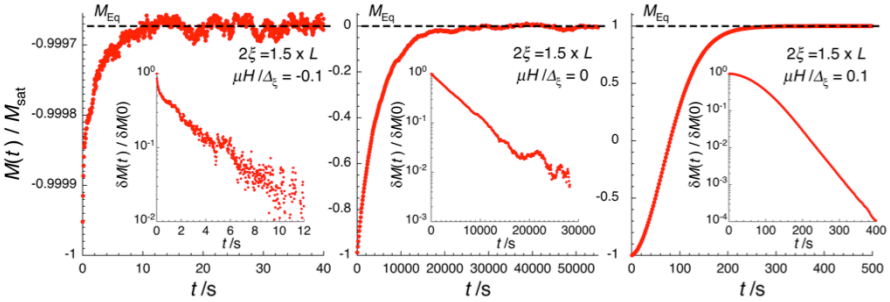

Figure 11. Relaxation of the normalized magnetization at a fixed temperature ($\Delta_\xi/k_BT = 5$) obtained by Monte Carlo simulations [35] in the finite-size regime ($2\xi > L$) starting from a completely saturated negative magnetization. The time decay of the reduced magnetization ($\delta M(t)/\delta M(0) = (M(t) - M(t \to \infty))/(M(t=0) - M(t \to \infty))$) in semilogarithmic plot is given in inset, (a) for a negative applied field ($\mu H/\Delta_\xi = -0.1$) (b) in absence of applied field ($\mu H/\Delta_\xi = 0$), (c) for a positive applied field ($\mu H/\Delta_\xi = 0.1$).

The presented relaxation curves are at the same temperature ($\Delta_\xi/k_BT = 5$) respectively for $H < 0$ (Fig. 11a), $H = 0$ (Fig. 11b) and $H > 0$ (Fig. 11c) and coherently in inset of these plots is given the time decay of the reduced magnetization ($\delta M(t)/\delta M(0) = M(t) - M(t \to \infty))/(M(t=0) - M(t \to \infty)$). The theoretical relaxation

of the magnetization under *dc* field is no longer a single exponential although a unique relaxation time can still be extracted at long time scale. As shown in Fig. 12, this deduced normalized relaxation time, τ/τ_0, is plotted as a function of the normalized inverse of the temperature (Δ_ξ/k_BT) and for different values of the normalized magnetic field ($\mu H/\Delta_\xi$) in order to evidence the different thermally activated regimes. As previously mentioned, only the correlation contribution to the relaxation time, τ/τ_0, is reported. Thus when the obtained activation energy, $\Delta_{\tau/\tau 0}$, is negative, it simply indicates that the activation energy for the relaxation time, Δ_τ, is smaller than Δ_A. In contrast with the obtained properties at zero (Fig. 9) or small applied fields, these numerical data suggest that, at higher fields, the temperature dependence of the relaxation time is strongly dependent of the introduced probability law (Fig. 12). This result is indeed expected since the previous argument of universality is no longer valid far from the critical point. From Fig. 12, the contribution of the activation energy due to the magnetic correlations, $\Delta_{\tau/\tau 0}$, can be deduced as a function of the applied magnetic field (Fig. 13). As already concluded from Fig. 12, very different activation energies are obtained for the three investigated probability laws for reduced magnetic fields, $\mu H/\Delta_\xi$. Moreover, the comparison between Monte Carlo simulations for $N = 100$ and numerical estimation with $N = 10$ using diagonalization of the dynamic linear equations (Eq. 13) allows to conclude that the obtained theoretical results are essentially independent of the chain length in the low temperature limit. These theoretical works strongly suggest that experimental dynamic properties under high applied magnetic fields should be able to specify the probability law that governs SCM systems. Such experiments are presently missing in the literature.

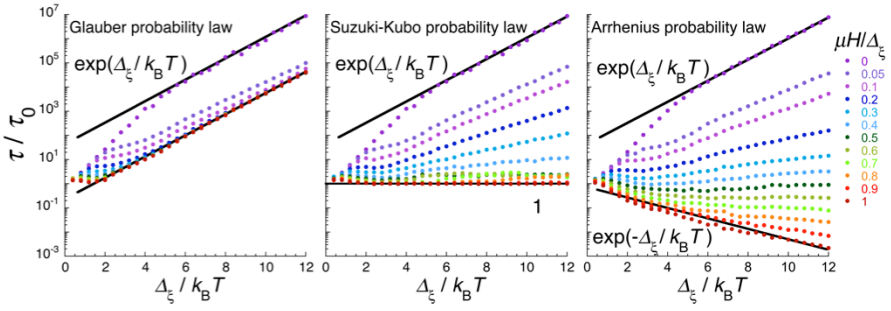

Figure 12. Normalized relaxation time as a function of the inverse of the normalized temperature determined by Monte Carlo simulations ($N = 100$)[35] for different values of the reduced magnetic field ($\mu H/\Delta_\xi$) in the case of (a) the Glauber, (b) Suzuki-Kubo, and (c) Arrhenius probability laws. Solid lines emphasize the low temperature activated regimes.

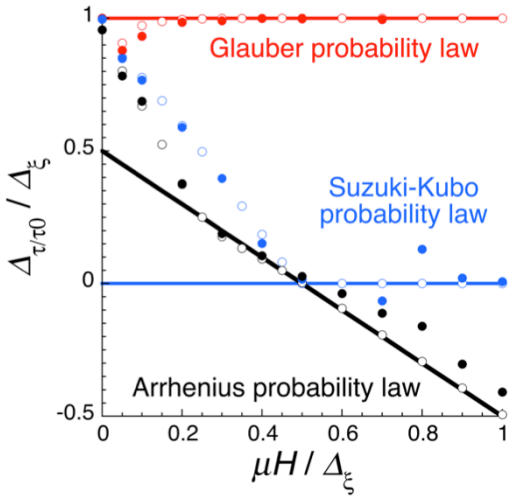

Figure 13. Variation of the normalized correlation activation energy, $\Delta_{\tau/\tau 0}/\Delta_\xi$, obtained at low temperature as a function of the reduced applied field, $\mu H/\Delta_\xi$ from numerical results for $N = 10$ (full diagonalization, open symbols) and for $N = 100$ (Monte Carlo approach; full symbols, from Fig. 12) in the case of the Glauber (red), Suzuki-Kubo (blue) and Arrhenius (black) probability laws. Solid lines emphasize the linear field dependence obtained at high field.

Experimentally, the effect of the applied *dc* field has been studied in details for only two different SCMs, including the [Mn_2Ni] chain [62]. As theoretically expected, the relaxation time of the magnetization is maximum in zero *dc* field and the low field critical regime is well reproduced. At larger fields, the experimental results suggest that the field dependence of τ_0 should be responsible for the limited variation of τ. Other perturbations, like the influence of interchain couplings, may also be relevant to discuss the field dependence of the relaxation time. As far as we know, reference 62 constitutes the only detailed study of a SCM under field in the literature. Obviously, more experimental work probing the influence of a *dc* field would certainly be useful to test the theoretical predictions summarized here and in particular to demonstrate if the SCMs follow or not a Glauber dynamics. It should be also mentioned that this type of study is essential to distinguish between systems exhibiting a 3-D magnetically ordered phase and a real SCM behavior (see section 4).

2.5 Quantum regime

In the previous subsections, the experimental results have been analyzed using classical models. Indeed as SCMs are mesoscopic objects, the influence of quan-

tum mechanics remains marginal for example in comparison with Single-Molecule Magnet systems. Quantum effects can however be observed and discussed at very low temperatures as long as a magnetic field is applied to lower the energy barrier [64,65]. In the case of the $[Mn_2Ni]$ chain chosen as the archetype SCM in this book chapter, the field sweep rate (v = dH/dt) and temperature dependence of the magnetization reversal has been studied below 2.6 K. The coercive or nucleation field, H_n, increases with decreasing temperature and increasing v as expected for a thermally activated process above 1 K. Below this temperature, H_n becomes temperature independent but remains strongly sweep rate dependent. This behavior and the detail analysis of the $H_n(v,T)$ data reveals that in this very low temperature region, the reversal of the magnetization is induced by a quantum nucleation of a domain wall that then propagates due to the applied field [64].

2.5.1
Quantum tunneling of the magnetization

As discussed previously, SCMs are built with spin units presenting, in general, a strong uniaxial anisotropy or in some cases SMM properties [66,67] like for instance in the case of the $[Mn_2Ni]$ chains. These 1-D coordination polymers result from the self-assembly of $[Mn_2(Rsaltmen)_2Ni(L_1)_2(L_2)_x]^{2+}$ moieties, which act individually as SMMs [68]. At low temperature, this SMM unit behaves like a giant $S = 3$ spin with a uniaxial magnetic anisotropy, D/k_B, equal to 2.5 K [15,26-28,68]. In a SMM, the strong uniaxial anisotropy creates an energy barrier, Δ_A, that can be overcome by temperature which in this case promotes spin reversal. This spin relaxation follows an Arrhenius law (Eq. 18) above a characteristic temperature, T^*. Below T^*, the classical magnetization dynamics becomes too slow and a faster mechanism of relaxation by quantum tunneling takes over.

Tunneling through a barrier is the archetypical effect of quantum mechanics. It happens when two states separated by an energy barrier are coupled and brought into resonance. The system can then tunnel from one state to the other.

A formal explanation of this mechanism is given by the Landau-Zener (LZ) theory. To illustrate this theory, a simple Hamiltonian given in Eq. 42, including rhombic magnetic anisotropy and Zeeman terms, should be considered (D and E being the longitudinal and transverse anisotropy, H_z the magnetic field along the z axis, and S_Z, S_+ and S_- the Pauli operators).

$$H = -DS_z^2 + E\left(S_+^2 + S_-^2\right) + g\mu_B\mu_0 H_z S_z \tag{42}$$

In the case of $E = 0$, the spin eigenstates are the m_S states (m_S = -3,…+3 for the $[Mn_2Ni]^{2+}$ SMMs) and then quantum tunneling is impossible since by definition eigenstates are stationary states. In the case of $E \neq 0$, S_+^2 and S_-^2 elements couple m_S states that satisfies the $\Delta m = \pm 2n$ rule (n being an integer number). In conse-

quence, when two coupled m_S states are brought into resonance (Fig. 14), the spin can tunnel from one state to the other. When the temperature increases and reaches the separation energy between two m_S states with $\Delta m = \pm 1$, the absorption of a phonon can promote the spin from the ground state to an excited state where tunneling through the barrier can occur (Fig. 14, b pathway). This phenomenon is called thermally assisted tunneling.

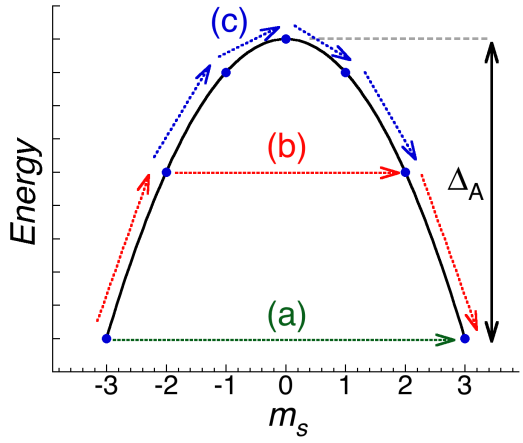

Figure 14. Representation of the different spin reversal mechanisms for an $S = 3$ SMM. The energy separating 0 from +3 states is the anisotropy barrier, Δ_A. It exists three possible mechanisms: (a) the system can tunnel directly through the barrier from m_S = -3 to +3, (b) the spin can be thermally promoted to an excited state and then tunnel, for example, from m_S = -2 to +2, it is the thermally assisted tunneling or (c) the spin gets enough thermal energy to pass over the energy barrier.

The tunneling probability between two states is given by the Landau-Zener probability, P_{LZ}, (Eq. 43; α is a coefficient that depends on the total spin number, Δ is the tunnel splitting that depends on the anisotropy parameters and v is the magnetic field sweep rate) [69].

$$P_{LZ} = 1 - \exp\left(-\alpha \frac{\Delta^2}{v}\right) \tag{43}$$

The LZ theory has been used to determine the different anisotropy parameters of SMMs [70] as well as to understand their quantum behavior such as quantum interferences [71,72]. In the following, we will describe how the LZ tunneling occurs and how it affects the magnetic behavior of SCM systems at very low temperature.

2.5.2
Nucleation of domain wall

At low temperature, a magnetic field can be applied in order to lower the energy barrier of a SCM system. When the field approaches a certain value, a domain wall can nucleate when a spin is reversed either by thermal activation or by quantum tunneling. Once triggered, the domain walls propagate due to the applied magnetic field, which induces a complete reversal of the SCM magnetization. Fig. 15 presents the field dependence of the magnetization for the [Mn_2Ni] chain at T = 1.4 K and 0.04 K for different sweep rates v. The nucleation field H_n corresponds here to the coercive field for which the magnetization reaches zero. Down to 0.5 K, H_n depends strongly on the temperature and the sweeping rate v that cannot be explained solely by the LZ theory.

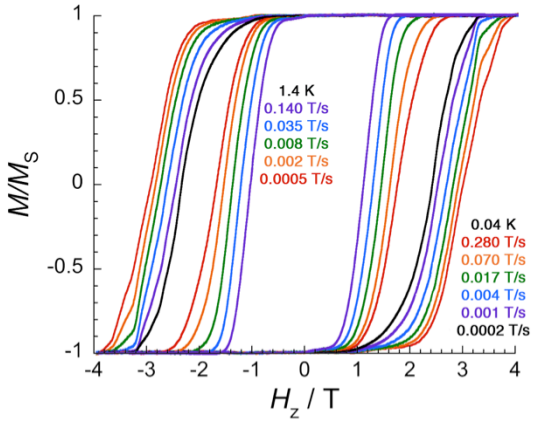

Figure 15. Field dependence of the magnetization on a single-crystal of $[Mn_2(saltmen)_2Ni(pao)_2(py)_2](ClO_4)_2$ at 1.4 K and 0.04 K. The magnetic field is applied along the easy magnetic direction, and the hysteresis loops are recorded at different sweep rates. Adapted from Ref. 64.

Indeed at a given magnetic field, the probability of having a nucleation induced by thermal fluctuations depends on how long the system stays at this field and hence depends on v. In order to discriminate between both regimes of nucleation (induced by thermal fluctuation versus LZ tunneling), Wernsdorfer et al. proposed a phenomenological law that has been successfully used to explain magnetization reversal at low temperature in various low dimensional magnetic systems [73,74]. The temperature and sweep rate dependence of the nucleation field is expressed by Eq. 44 in which H_n^0 is the nucleation field at T = 0 K, E_0 the energy barrier and b a constant that depends on the Arrhenius prefactor of Eq. 25 .

$$H_n \approx H_n^0 \left(1 - \sqrt{\frac{k_B T}{E_0} \ln\left(\frac{b}{v}\right)} \right) \tag{44}$$

Measuring the nucleation field for different sweep rates at different temperatures allows to plot H_n as a function of a reduced variable $(T \ln(b/v)/E_0)^{1/2}$ in Fig. 16a. These experimental plots show that above 1 K all the data points collapse on a single master curve. The deviation from this regime at lower temperatures reveals LZ quantum tunneling. As introduced in the previous section, the LZ probability is independent of the temperature. As a result, when replacing T by an effective temperature T_{eff} that is constant below 1 K, all experimental data now collapse on the same master curve shown Fig.16b. This behavior is unequivocally the signature of quantum nucleation of domain walls [64].

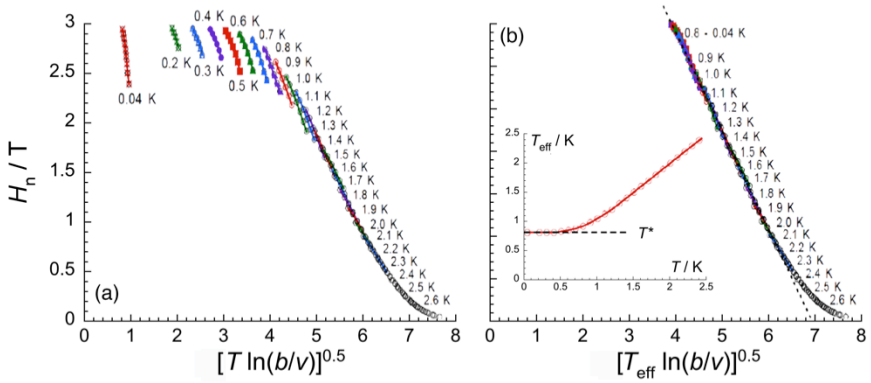

Figure 16. Scaling plots of the nucleation field H_n for $[Mn_2(saltmen)_2Ni(pao)_2(py)_2](ClO_4)_2$ for different sweep rates (a) at different temperatures and (b) at different effective temperature T_{eff}. The inset gives T_{eff} as a function of T. Adapted from Ref. 64.

This phenomenological approach highlights the key role of LZ tunneling in the nucleation of the domain walls at very low temperature in SCM systems [64,65]. However, a unified theory is still missing to fully describe the SCM dynamic at very low temperatures. Moreover, extended experiments in which the tunnel splitting Δ is tuned through the modification of the transverse anisotropy or the application of a transverse field would certainly improve the understanding of quantum nucleation of domain walls in SCMs.

3
Regular chain of antiferromagnetically coupled anisotropic spins

For most of the magnetic problems, the only difference between ferromagnetic and antiferromagnetic cases is simply the sign of the exchange constant. Hence the duality of the two systems allows to directly transpose the theoretical results obtained in the ferromagnetic case to the antiferromagnetic one. This very general rule can of course be applied to the regular chain of magnetically coupled anisotropic spins transposing the results obtained for the ferromagnetic case in the previous sections to the antiferromagnetic case that will be described in the following paragraphs.

3.1
Infinite chain length regime

3.1.1
Static properties

As expected, the equilibrium properties of the antiferromagnetic and ferromagnetic chain models are the same and a simple change of the interaction sign is necessary. As a result, the net magnetization of the ground state is zero but the magnetization oscillates in space, i.e. staggered magnetization, with a wave vector $q_0 = \pi/a$ (where a is the unit cell parameter; Fig. 17a). In the low temperature limit, the equilibrium state consists of large oriented magnetic domains separated by narrower domain walls (Fig. 17b). Therefore for decreasing temperature, the parallel susceptibility in zero field decreases exponentially and the response for a polycrystalline sample is given by Eq. 45 in the Ising limit. This relation can be generalized beyond the Ising limit by Eq. 46.

$$\chi = \frac{2}{3}\chi_{\perp} + \frac{C}{3T}\exp\left(-4|J|S^2/k_BT\right) \tag{45}$$

$$\chi = \frac{2}{3}\chi_{\perp} + \frac{C}{3T}\exp\left(-\Delta_{\xi}/k_BT\right) \tag{46}$$

Nevertheless, an essential difference appears in these relations. As the parallel component of the susceptibility decreases exponentially, the transverse contribu-

tion is no longer negligible (like it was in the ferromagnetic case, Eq. 4) and therefore this parameter should be introduced in the fitting procedure of experimental data on polycrystalline samples. In the antiferromagnetic case, the correlation length is still diverging at low temperature but the corresponding susceptibility is now the response to a "staggered magnetic field", i.e. to a field which oscillates in space with a wave vector $q_0 = \pi/a$. The staggered susceptibility, $\chi(q_0)$, describes the response to a staggered magnetic field and is thus proportional to the correlation length as shown by Eq. 47.

$$\frac{\chi(q_0)T}{C} = \frac{2\xi}{a} \tag{47}$$

Eq. 47 is the strict equivalent of Eq. 3 found for the static susceptibility in the ferromagnetic case. The expression of the correlation length is given by Eq. 48 and Eq. 49 in the Ising limit and in the general case respectively.

$$\frac{\xi}{a} = \exp\left(4|J|S^2/k_BT\right) \tag{48}$$

$$\frac{\xi}{a} = \exp\left(\Delta_\xi/k_BT\right) \tag{49}$$

3.1.2 Dynamic properties

To make the parallel with the ferromagnetic case, it should be realized that the slow relaxation in chains of antiferromagnetically coupled spins concerns the relaxation of the staggered magnetization (Fig. 17a). On the other hand, the static magnetization relaxes even more quickly than for non-interacting spins. For the relaxation of this mode ($q_0 = \pi/a$), the expression of the relaxation time given in Eq. 50 is exactly the same as the one found for an infinite chain of ferromagnetically coupled spins (Eq. 19).

$$\tau(q_0) = \frac{\tau_i}{2}\exp\left(\left(2\Delta_\xi + \Delta_A\right)/k_BT\right) \tag{50}$$

However, as the static susceptibility probes the relaxation of the uniform magnetization ($q = 0$), this kind of measurement is not appropriate to study the slow relaxation in the antiferromagnetic case. Note that experimentally the staggered mag-

netization can be deduced from the NMR relaxation time. This method has been extensively used to study organic conductors and probe the occurrence of a 3-D antiferromagnetic order [75].

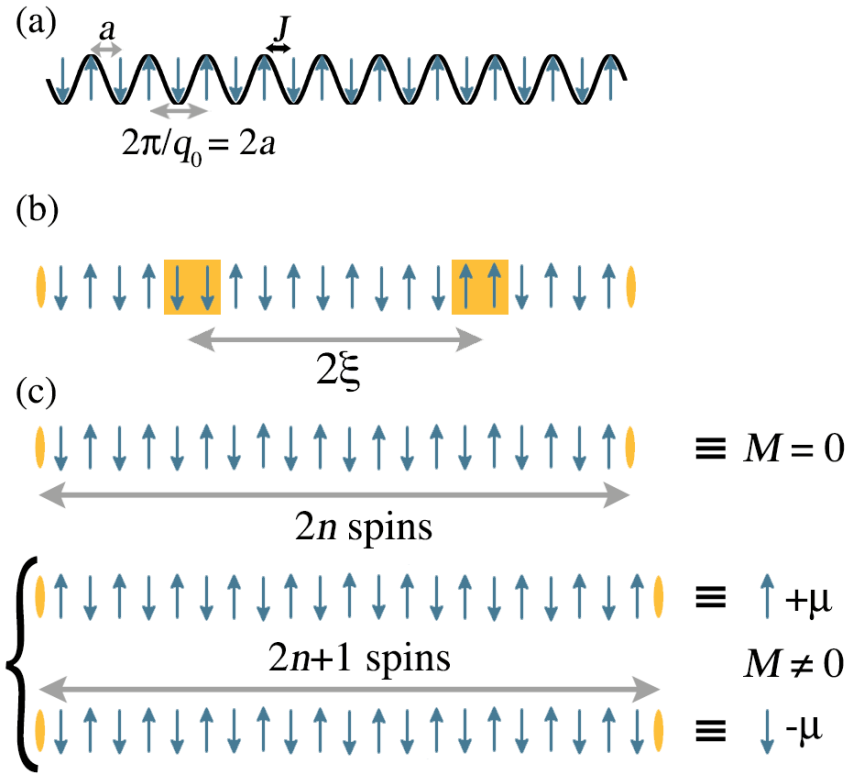

Figure 17. Schematic views of a chain of antiferromagnetically coupled Ising-type spins in zero-*dc* field: (a) the representation of the ground state (staggered magnetization: sinusoid black line); at a finite temperature in the cases of (b) $2\xi < L$ and (c) $2\xi >> L$ (L is the distance between two defects, i.e. orange ellipses).

3.2
Finite size regime

3.2.1
Static properties

As for the ferromagnetic case, the magnetic susceptibility of a finite chain can be exactly obtained [50,51] and the same expression of the parallel susceptibility can

be used (Eq. 21) for antiferromagnetic interactions ($J < 0$). A simplified expression of $\chi T/C$, Eq. 51, is obtained at low temperature when c, the number of defects, is small. At this approximation, the average susceptibility for polycrystalline samples is given by Eq. 52.

$$\frac{\chi_{//}T}{C} = \frac{c + 2\exp\left(-4|J|S^2/k_BT\right)}{2} \tag{51}$$

$$\chi = \frac{C}{3T}\left(\frac{c + 2\exp\left(-4|J|S^2/k_BT\right)}{2}\right) + \frac{2}{3}\chi_{\perp} \tag{52}$$

At low temperature, the parallel susceptibility saturates to a limit value given by Eq. 53.

$$\frac{\chi_{//}T}{C} = \frac{c}{2} \tag{53}$$

Indeed, this result can be easily understood. In a polydisperse description, segments of all sizes are found (Fig 17c). For those containing an odd number of spins, a non-compensated magnetization equal to the magnetic moment of one spin unit is found, independently of the length of the segment. The percentage of defects associated with odd segments is in fact $c/2$, which gives directly the Curie component written above. It is worth to emphasize in this case that the monodisperse description would be artificial as the statistic of segment lengths becomes at low temperature a major contribution of the magnetic susceptibility (Eq. 51-53).

3.2.2
Dynamic properties

As for the infinite chain (section 3.1.2), the expression of the relaxation time for the staggered magnetization in the finite size regime, Eq. 54, can be deduced from the ferromagnetic case (Eq. 25).

$$\tau\left(q_0\right) = \frac{\tau_i L}{2a}\exp\left(\left(\Delta_\xi + \Delta_A\right)/k_BT\right) \tag{54}$$

Remarkably, the dynamics of the finite chain of antiferromagnetically coupled spins can be observed even by standard M versus *time* or *ac* measurements. Fig.

17c describes schematically the reversal of the staggered magnetization of an odd segment at low temperature. The net magnetization of these segments goes from $+\mu$ to $-\mu$ between the initial and final states. Then the total magnetization of the material changes with time and a mode can be detected with the *ac* susceptibility with however a weak intensity proportional to the number of defects. It is astonishing to realize that the dynamics of these chains is detected only in finite size regime ($2\xi > L$) thanks to the defects present in the system. This argument has obviously no counterpart in the infinite chain case ($2\xi < L$).

It exists in the literature experimental data illustrating these arguments in three different materials containing one-dimensional coordination polymer of $S = 9$ $[Mn_4(hmp)_6]^{4+}$ SMMs [29,30]: $[Mn_4(hmp)_6(L)_2](ClO_4)_2$; L^-: N_3^-, CH_3COO^-, $ClCH_2COO^-$. The amount of defects has been deduced from the modeling of the static magnetic susceptibility as described in the previous paragraph (3.2.1). As expected from the theory, the activation energy deduced for the temperature dependence of the relaxation time is consistent only with finite chains and not with the expected intrinsic dynamics of the isolated SMM units. Finally, the polydisperse character of these systems has also been emphasized through the characteristic asymmetric shape of the Cole-Cole plots and the non-exponential decay of the magnetization [29] in coherence with the theoretical prediction of reference 53 (Fig. 18).

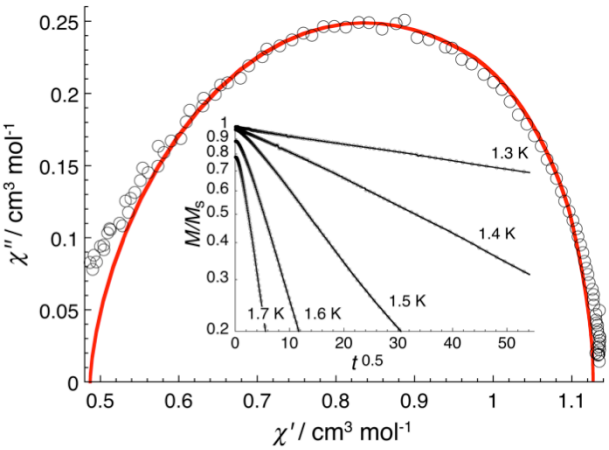

Figure 18. Cole-Cole plot deduced from the *ac* susceptibility components at 2.7 K for $[Mn_4(hmp)_6(N_3)_2](ClO_4)_2$. The solid line gives the theoretical prediction from the polydisperse model [29,53]. Inset: selected *M* versus *time* data plotted as a function of $t^{0.5}$ to emphasize the non-exponential relaxation of the magnetization. Adapted from Ref. 29.

4
From SCM to 3D ordered systems

It was previously believed that the slow relaxation of the magnetization observed for SMM or SCM systems no longer exists if a 3-D magnetic order is present. For this reason, many systems have been described in the literature as SCMs based solely on zero field magnetic data, as soon as a slow dynamics was evidenced for example by *ac* susceptibility measurements. However, it has been recently demonstrated, both experimentally and theoretically, that slow relaxation of the magnetization and 3-D antiferromagnetic order can coexist [31,32,33].
As interchain couplings are antiferromagnetic in most of the cases, the simplest system, that generalizes the discussion made in section 2, corresponds to ferromagnetically coupled anisotropic spins organized in regular chains, which antiferromagnetically interact. Experimentally, the simultaneous presence of a 3-D antiferromagnetic order and a slow relaxation of the magnetization have been clearly demonstrated for the first time in $[Mn_2(5\text{-MeOsaltmen})_2Ni(pao)_2(phen)](PF_6)_2$ that is composed of the same type of $[Mn_2Ni]$ chain described in section 2. The essential difference between the different $[Mn_2Ni]$ chain based compounds resides only in the magnitude of the antiferromagnetic interchain couplings. When strong enough, these interactions induce a 3-D antiferromagnetic order without destroying the intrinsic slow dynamics of the chains. Like in the rest of this book chapter, the $[Mn_2Ni]$ chain system will be used as an example to illustrate the theoretical arguments given in this section.

4.1
Static properties

Fig. 19a shows the χT product obtained on a polycristalline sample for different (low) values of the applied magnetic field. Above 5 K, the χT value is independent of the *dc* field and clearly thermally activated as expected for SCM (Eq. 3, Fig. 6). However at lower temperatures, the strong field dependence of the susceptibility and its noticeable decrease in zero *dc* field are characteristic of a 3-D antiferromagnetic ordered state.

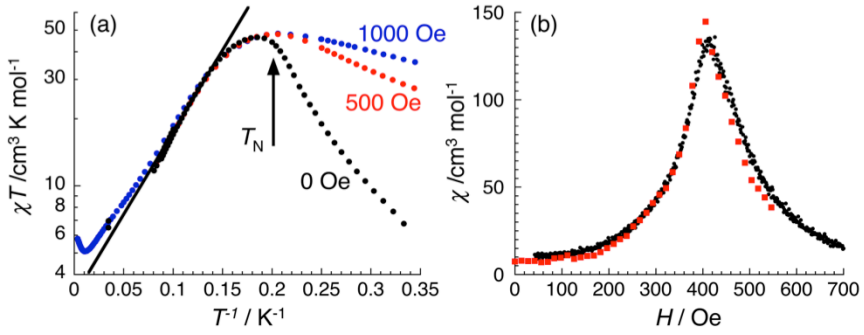

Figure 19. Experimental data for $[Mn_2(5\text{-MeOsaltmen})_2Ni(pao)_2(phen)_2](PF_6)_2$ (with 5-MeOsaltmen and phen being the *N,N'*-(1,1,2,2-tetramethylethylene) bis(5-methoxy salicylideneiminate) and 1,10-phenanthroline ligands) : (a) magnetic susceptibility data on a polycrystalline sample at different applied fields; (b) field dependence of the single crystal susceptibility deduced from magnetization measurements at 2.9 K (black dots) with a field sweeping rate of 22 Oe/s. The susceptibility deduced from relaxation data after normalization is also shown (red squares). Adapted from Ref. 31.

At the same time, experiments on an oriented single-crystal (Fig. 19b) show that the maximum of the susceptibility (dM/dH), at a given temperature, occurs at a finite field, H_C, of about 400 Oe while theoretically, it should be located at $H = 0$ for a SCM (Eq. 28 and 30). Consistent results were obtained on oriented single crystals and polycrystalline samples. It is worth mentioning that the maximum of susceptibility on polycrystalline samples is, in theory, always slightly higher (by a factor of about 1.15) than H_C accurately obtained from single-crystal measurements (see supporting information of Ref. 31).

These static magnetic properties have been analyzed in the frame of a simple model for which antiferromagnetic interchain interactions are introduced and treated within the mean field approximation. The resulting phase diagram is given in Fig. 20 with a comparison between experimental and theoretical results. The theory specifies the existence of two characteristic fields: (i) a critical field, H_C, associated to the antiferromagnetic-paramagnetic phase transition and (ii) an inversion field H_{inv}, located in the antiferromagnetic phase, which corresponds to the cancelation of the magnetization of one of the two sublattices. Both fields are temperature dependent and vanish at T_N, the transition temperature at zero field (Fig. 20). The temperature dependence of H_C can be followed experimentally from the maximum of dM/dH and is perfectly in agreement with the theory.

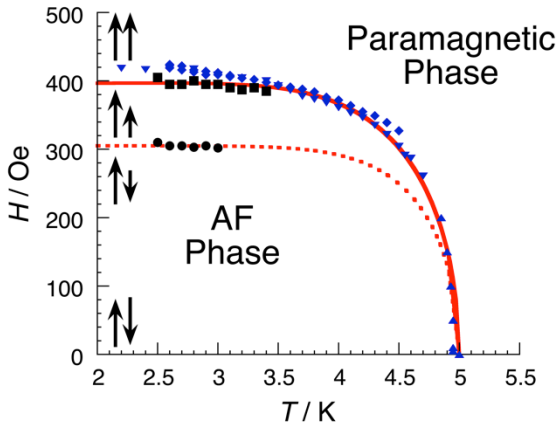

Figure 20. Phase diagram for $[Mn_2(5\text{-MeOsaltmen})_2Ni(pao)_2(phen)_2](PF_6)_2$. Position of the susceptibility maximum from the *M* versus *H* data: (◆) single crystal, (▼) powder measurements; or from the temperature dependence of the powder *ac* susceptibility at a given *dc* field (▲). Experimental points deduced from the dynamics measurements, (■) location on the main maximum of the relaxation time and (●) location of the second maximum (inversion point). The continuous line is the theoretical predictions of the antiferromagnetic - paramagnetic phase transition and the dashed line gives the line of inversion points. The arrows are schematizing the orientation and magnitude of the two order parameters of the problem. Adapted from Ref. 31.

The magnitude of the interchain coupling can be deduced from the extrapolation of H_C at zero temperature, while T_N depends both on the intrachain correlation length and the interchain couplings. As the intrachain correlation length can be estimated independently from the temperature dependence of the χT product in the paramagnetic phase (Fig. 6 or 19a), the consistency between the experiment and the theoretical analysis can be completely verified.

To conclude, it should be mentioned that the inversion and critical fields are small as they essentially correspond to the situation where the external field (i.e. the Zeeman energy, which draws all chains in the same orientation) compensates the small interchain coupling (which favors the antiferromagnetic order of the chains). As soon as the interchain coupling is small, these magnetic fields are small and the system remains strongly influenced by the intrinsic single chain properties. This argument can also be applied to the dynamic properties as it is shown in the following subsection.

4.2
Dynamic properties

The dynamic properties of this $[Mn_2Ni]$ compound have also been studied and analyzed [31]. Strictly speaking, the relaxation of the magnetization is no longer fol-

lowing a simple single exponential law when a magnetic field is applied. Nevertheless for a first analysis, the characteristic time has been deduced considering $M(t)$ data measured on single crystals and taking the time where the normalized magnetization is equal to 1/e. Fig. 21 shows the field dependence of the deduced relaxation time at two different temperatures.

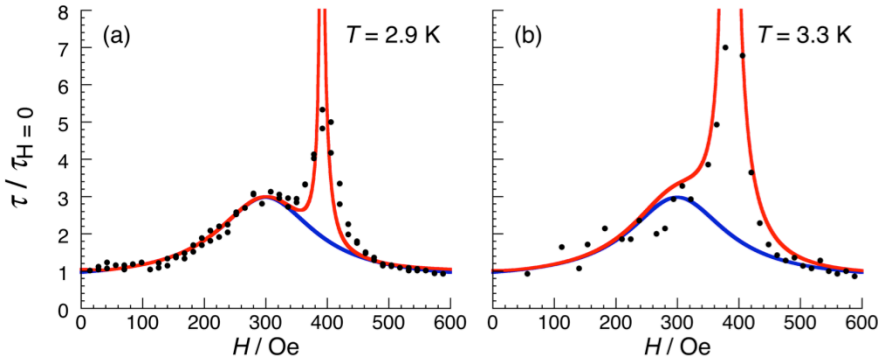

Figure 21. Field dependence of the deduced relaxation time (normalized at zero field) for $[Mn_2(5\text{-MeOsaltmen})_2Ni(pao)_2(phen)_2](PF_6)_2$: black dots (a) at T = 2.9 K, (b) at T = 3.3 K. The blue line shows the expected relaxation time when the magnetization m_1 of the sublattice #1 is saturated. The continuous line gives the calculated relaxation time using a mean field approach. Adapted from Ref. 31.

A maximum of the relaxation time is no longer obtained at zero field as expected for SCMs (Eq. 38-41). On the other hand, it reaches a maximum close to the critical field H_C (Fig. 19b and 21). Nevertheless, a thermally activated behavior of the relaxation time is still observed with an activation energy consistent with the infinite chain regime of a SCM (Eq. 19). As a consequence, it should be emphasized that the plot of $\ln(\tau)$ versus $1/T$ does not really help to make the difference between a real SCM and a sample exhibiting both slow relaxation of the magnetization and a 3-D antiferromagnetically ordered system. This remark highlights the key importance of the field dependence of the relaxation time to discriminate between the two magnetic states.

The mean field theory used to describe the static properties (Fig. 20) was also applied to analyze these dynamic results. Although it may be too simple (in particular the non-exponential relaxation of the magnetization is not described in this approximation), this first theoretical approach shows that slow relaxation of the magnetization and 3-D antiferromagnetically order are not incompatible and can coexist. Moreover a good agreement between the mean-field theory and the experimental results was obtained as illustrated in Fig. 21.

To conclude this section, we should emphasize that many compounds have been described as SCMs based only on studies performed in zero *dc* field. Indeed, this section underlines that in these experimental conditions, it is difficult to make the difference between real SCM properties and a magnetic behavior that implies a

long range ordered magnetic ground state. This is the reason why in the literature many materials were described erroneously as SCMs.

5
Conclusions and opened questions

In this book chapter, SCMs with simple spin architectures have been described on a theoretical point of views and illustrated by selected experimental data. Nevertheless, one-dimensional magnetic systems with a more complex spin and interaction topologies have also been synthetized and are, indeed, the most common in the literature. In all these cases, the theory is much less developed as both static and dynamic properties are more complicated to describe.
In any case, as soon as some Ising-type magnetic anisotropy is present, the low temperature properties are always strongly influenced by the presence of domain walls. As a consequence, the first step to understand static and dynamic properties is certainly to specify the structure of these domain walls. As shown in section 2.2.1 for a regular chain of ferromagnetically coupled anisotropic spins, narrow profiles are always found as soon as $D/J > 4/3$. A recent theoretical work shows a more complicated scenario as soon as the chain topology becomes more complex [35]. To illustrate this argument, two examples shown in Fig. 22 have been selected: (a) a chain composed of an alternation of isotropic *s* spins and anisotropic *S* spins in antiferromagnetic interactions and (b) a chain of canted anisotropic spins.

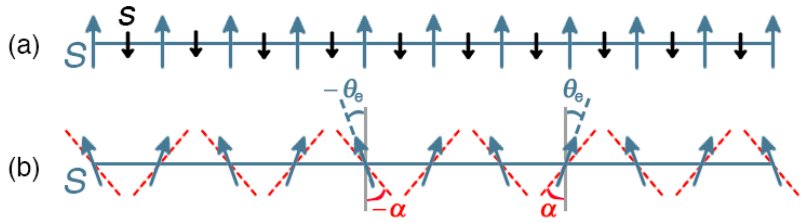

Figure 22. Schematic representation of the structure of more complex chains: (a) a mixed ferrimagnetic chain composed of an alternation of isotropic (black) and anisotropic (blue) spins and (b) a canted chain where an alternation of the easy axis orientation is found (defining the α angle). In the latter case, the easy axes are visualized by red dashed lines. The spins are oriented in the direction of equilibrium (defining θ_e for in the (b) case) in absence of domain walls.

For the chain with a ferrimagnetic spin topology, Fig. 23a gives the calculated angle, θ_0, of the first spin located in the right part of the domain wall, as a function of the anisotropy-exchange energy ratio ($DS/2Js$). These theoretical data can be readily compared with their analogues for the regular chain (Fig. 5a). The striking difference is that strictly narrow domain walls no longer exist.

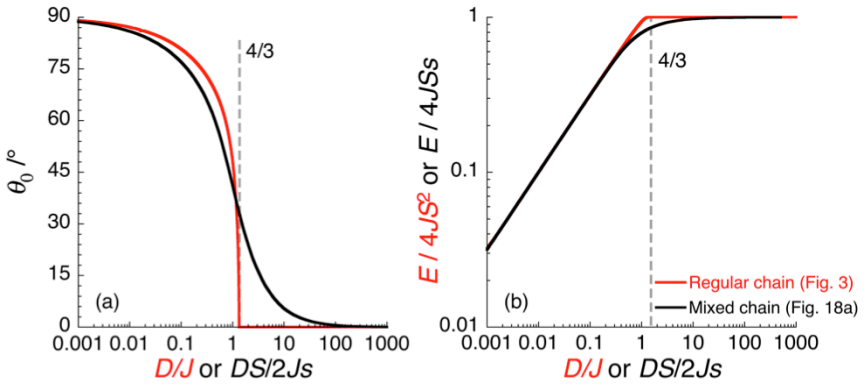

Figure 23. (a) Variation of the equilibrium angle of the $n = 0$ spin, θ_0 and (b) the corresponding normalized energy, E, of the domain wall as a function of the anisotropy-exchange energy ratio, for the mixed chain (Fig. 22a; black line) compared to the regular chain of ferromagnetically coupled spins (Fig. 3; red line). For a better comparison, the energy of the mixed chain is normalized by $4JSs$ (instead of $4JS^2$ for the regular chain) and D/J has been multiplied by $S/2s$ for the mixed chain to obtain a superposition of the two curves in the broad and Ising limits.

For any value of $DS/2Js$, the width of the domain wall is larger than a simple unit cell. This result points out that the transition observed at $D/J = 4/3$ for the regular chain does not exist anymore for this type of "ferrimagnetic" chains (Fig. 22a). The same conclusions can be drawn from the variation of the domain wall energy (Fig. 23b), that does not show any cusp at any value of $DS/2Js$.

Similar theoretical data on the domain wall are also available for a chain of canted anisotropic spins (Fig. 22b). In this case, two different angles should be introduced to characterize the profile of a domain wall, each of them having a non zero equilibrium value. Therefore to specify the topology of the domain wall in this case, it is easier to use a single angular parameter, $\delta\theta_0$, obtained from the subtraction of this equilibrium value, θ_e, to the angle, θ_0, (the angle of the first spin located in the right part of the domain wall). Fig. 24a reports the variation of $\delta\theta_0 = \theta_0 - \theta_e$ (Fig. 22b) as a function of D/J. As for the previous type of chain, the transition observed at $D/J = 4/3$ for the regular chain (Fig. 5) is also suppressed when introducing any value of the canting angle (α, Fig. 22b) and thus strictly narrow domain walls no longer exist. Fig. 24b gives the corresponding calculated energy of the domain wall that has been normalized to $4JS^2\cos(2\alpha)$, the expected value of this energy in the Ising limit. These theoretical data show that the Ising limit is only reached for very large values of D/J as α increases. This limit is thus inappropriate to describe most of real systems. Moreover, a unique limit is found for small values of D/J when this ratio is normalized by $\cos(2\alpha)$, showing that $J\cos(2\alpha)$ plays the role of an effective exchange energy in this case.

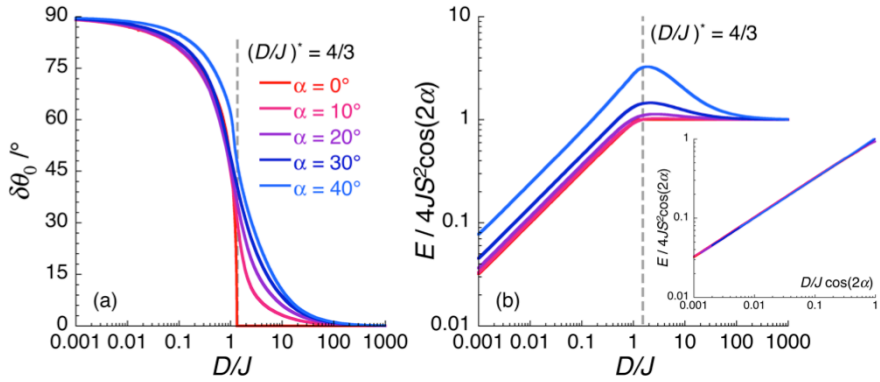

Figure 24. (a) Variation of the differential angle, $\delta\theta_0 = \theta_0 - \theta_e$, and (b) the corresponding normalized energy of the domain wall as a function of D/J (Inset: as a function of the $D/J\cos(2\alpha)$) for the canted chain (Fig. 22b) compared to the regular chain ($\alpha = 0°$) of ferromagnetically coupled spins (Fig. 3 and 5; red line).

These selected results highlight that novel and original results are expected from one-dimensional magnetic systems with more complex spin and interaction topologies. However, either theoretical or experimental data on such systems remain very preliminary. In particular, this book chapter shows that magnetic experiments should explore the temperature and field dependence of both static and dynamic properties for a detailed and convincing analysis. Returning to the simple "ferromagnetic" chain described in section 2, it should also be emphasized that the SCM properties in the broad domain wall limit (i.e. $D/J << 4/3$) is far from being completely understood. In this regime, other excitations, like spin-waves should compete with domain walls at finite temperature and both static and dynamic properties are certainly more difficult to understand. On the other hand, we have shown that the properties of the SCMs in the narrow domain wall limit ($D/J > 4/3$) are more accessible, but even in this case, a lot of work remains to be done. For example, experimental results at "high *dc* field" (section 2.4) are still missing to discriminate between the different possible probability laws in contrast with the universal results obtained near the critical point (i.e. near $T = 0$ and $H = 0$).

To conclude this book chapter, it appears important to reinforce the idea of the universality of the physics near this critical point. This strongly suggests that the relations between the different activation energies obtained at zero field: $\Delta_{\tau 1} = 2\Delta_\xi + \Delta_A$ and $\Delta_{\tau 2} = \Delta_\xi + \Delta_A$, must be valid, at least for large values of the anisotropy energy and at low temperature. As these relations were deduced from general scaling arguments, they can probably be transposed to more exotic chains. Following the same idea, the critical regime obtained at low field is expected to be universal. On the other hand, results at higher *dc* fields should be more sensitive to the spin and interaction topologies of the chain. This part of the problem remains also unexplored, both theoretically and experimentally.

Last but not least, it was remarkable to discover that the SCM behavior is preserved for systems exhibiting a long range magnetic order, at least when the interchain couplings are weaker than the intrachain interactions. This result opens the possibility to prepare new quasi one-dimensional compounds presenting slow relaxation of the magnetization at higher temperature. But at the same time, the experimentalist is now forced to perform detailed magnetic studies and analyses (with and without applying a magnetic field) to fully characterize a potential SCM and more importantly to differentiate between a true SCM systems and a 3-D magnetic order. In this respect, it would probably be useful to reinvestigate with critical eyes some published systems described as SCMs based only on a limited amount of experimental results.

Acknowledgements

We are grateful to all our co-workers, past students and friends who have contributed to our scientific adventures. In addition, the authors thanks the Conseil Régional d'Aquitaine, the Université of Bordeaux, the CNRS and the ANR.

References

[1] Boyd PDW, Li Q, Vincent JB, Folting K, Chang H-R, Streib WE, Huffman JC, Christou G, Hendrickson DN (1988) J. Am. Chem. Soc. 110:8537
[2] Caneschi A, Gatteschi D, Sessoli R (1991) J. Am. Chem. Soc. 113:5873
[3] Sessoli R, Tsai H-L, Schake AR, Wang S, Vincent JB, Folting K, Gatteschi D, Christou G, Hendrickson DN (1993) J. Am. Chem. Soc. 115:1804
[4] Sessoli R, Gatteschi D, Caneschi A, Novak MA (1993) Nature 365:141
[5] Thomas L, Lionti F, Ballou R, Gatteschi D, Sessoli R, Barbara B (1996) Nature 383:145
[6] Gatteschi D, Sessoli R, Villain J (2006) Molecular Nanomagnets, Oxford University Press, Oxford.
[7] Pedersen KS, Bendix J, Clérac R (2014) Chem. Commun. 50:4396
[8] Leuenberger MN, Loss D (2001) Nature 410:789
[9] Bogani L, Wernsdorfer W (2008) Nature Materials 7:179
[10] Afronte M (2008) J. Mater. Chem. 19:1731
[11] Winpenny REP (2008) Angew. Chem. Int. Ed. 47:7992
[12] Wernsdorfer W (2008) C. R. Chimie 11:1086
[13] Mannini M, Pineider F, Sainctavit P, Danieli C, Otero E, Sciancalepore C, Talarico AM, Arrio MA, Cornia A, Gatteschi D, Sessoli R (2009) Nature Materials 8:194
[14] Caneschi A, Gatteschi D, Lalioti N, Sangregorio C, Sessoli R, Venturi G, Vindigni A, Rettori A, Pini MG, Novak MA (2001) Angew. Chem. Int. Ed. 40:1760
[15] Clérac R, Miyasaka H, Yamashita M, Coulon C (2002) J. Am. Chem. Soc. 124:12837
[16] Coulon C, Miyasaka H, Clérac R (2006) Struct. Bonding 122:163
[17] Miyasaka H, Clérac R (2005) Bull. Chem. Soc. Jpn 78:1725
[18] Xu G, Wang Q, Liao D, Yang G (2005) Prog. Chem. 17:970
[19] Lescouëzec R, Toma LM, Vaissermann J, Verdaguer M, Delgado FS, Ruiz-Pérez C, Lloret F, Julve M (2005) Coord. Chem. Rev. 249:2691
[20] Bogani L, Vindigni A, Sessoli R, Gatteschi D (2008) J. Mater. Chem. 18:4750
[21] Miyasaka H, Julve M, Yamashita M, Clérac R (2009) Inorg. Chem. 48:3420
[22] Brooker S, Kitchen JA (2009) Dalton Trans. 7331
[23] Sun H-L, Wang Z-M, Gao S (2010) Coord. Chem. Rev. 254:1081
[24] Zhang W-X, Ishikawa R, Breedlove B, Yamashita M (2013) 3:3772
[25] Glauber J (1963) J. Math. Physics 4:294
[26] Miyasaka H, Clérac R, Mizushima K, Sugiura K, Yamashita M, Wernsdorfer W, Coulon C (2003) Inorg. Chem. 42:8203
[27] Saitoh A, Miyasaka H, Yamashita M, Clérac R (2007) J. Mater. Chem. 17:2002
[28] Miyasaka H, Saitoh A, Yamashita M, Clérac R (2008) Dalton Trans. 2422
[29] Lecren L, Roubeau O, Coulon C, Li Y-G, Le Goff XF, Wernsdorfer W, Miyasaka H, Clérac R (2005) J. Am. Chem. Soc. 127:17353
[30] Lecren L, Roubeau O, Li Y-G, Le Goff XF, Miyasaka H, Richard F, Wernsdorfer W, Coulon C, Clérac R (2008) Dalton Trans. 755
[31] Coulon C, Clérac R, Wernsdorfer W, Colin T, Miyasaka H (2009) Phys. Rev. Lett. 102:167204
[32] Miyasaka H, Takayama K, Saitoh A, Furukawa S, Yamashita M, Clérac R (2010) Chem. Eur. J. 16:3656
[33] Bhowmick I, Hillard EA, Dechambenoit P, Coulon C, Harris TD, Clérac R (2012) Chem. Commun. 48:9717
[34] Barbara B (1994) J. Magn. Magn. Mat. 129:79
[35] Coulon C, Pianet V *unpublished results*
[36] Lajzerowicz J, Niez JJ (1979) J. Physique Lett. 40:L165

[37] Fisher ME (1964) Am. J. Phys. 32:343. A general demonstration of the relation between the correlation length and the zero-field magnetic susceptibility is made by Fisher this reference. His demonstration is then applied to the classical Heisenberg model.
[38] Nakamura K, Sasada T (1978) J. Phys. C 11:331.
[39] Nakamura K, Sasada T (1977) Solid State Commun. 21:891.
[40] Sakai T, Matsumoto M, Asakura K, Sato M (2005) Prog. Theo. Phys. Supplement 159:308
[41] Billoni, O, Pianet V, Pescia D, Vindigni A (2011) Phys. Rev. B 84:064415
[42] Coulon C, Clérac R, Lecren L, Wernsdorfer W, Miyasaka H (2004) Phys. Rev. B 69:132408
[43] Cole KS, Cole RH (1941) J. Chem. Phys. 9:341
[44] Clérac R *unpublished results*
[45] Sun Z-M, Prosvirin AV, Zhao H-H, Mao J-G, Dunbar KR (2005) J. Appl. Phys. 97:10B305
[46] Huang HW (1973) Phys. Rev. A 8:2553
[47] Saito Y, Kubo R (1976) Journ. Stat. Phys. 15:233
[48] Boukheddaden K, Shteto I, Hoo B, Varret F (200) Phys Rev B 62:14806
[49] Cordery R, Sarker S, Tobochnik J (1981) Phys Rev B 24:5402
[50] Wortis M (1974) Phys. Rev. B 10:4665
[51] Matsubara F, Yoshimura K (1973) Can. J. Phys. 51:1053
[52] Luscombe JH, Luban M, Reynolds JP (1996) Phys. Rev. E 53:5852
[53] Dhar D, Barma M (1980) Journ. Stat. Phys. 22:259
[54] Schwarz G (1965) J. Mol. Biol. **11**:64
[55] Pipkin AC, Gibbs JH (1996) Biopolymers 4:3
[56] Craig ME, Crothers DM (1968) Biopolymers 6:385
[57] Schwarz G (1968) Biopolymers 6:873
[58] Schwarz G (1968) Rev. Mod. Phys. 40:206
[59] Schwarz G (1972) J. Theor. Biol. 36:569
[60] Schwarz Jr M, Poland D (1976) J. Chem. Phys. 65:2620
[61] Baumgärtner A, Binder K (1979) J. Chem. Phys. 70:429
[62] Coulon C, Clérac R, Wernsdorfer W, Colin T, Saitoh A, Motokawa N, Miyasaka H (2007) Phys. Rev. B 76:214422
[63] Suzuki M, Kubo R (1968) J. Phys. Soc. Jap. 24:51
[64] Wernsdorfer W, Clérac R, Coulon C, Lecren L, Miyasaka H (2005) Phys. Rev. Lett. 95:237203
[65] Toma LM, Lescouëzec R, Pasan J, Ruiz-Perez C, Vaissermann J, Cano J, Carrasco R, Wernsdorfer W, Lloret F, Julve M (2006) J. Am. Chem. Soc. 128:4842
[66] Roubeau O, Clérac R (2008) Eur. J. Inorg. Chem. 4313:4480
[67] Jeon IR, Clérac R (2012) Dalton Trans. 41:9569
[68] Miyasaka H, Nezu T, Sugimoto K, Sugiura K-i, Yamashita M, Clérac R (2005) Chem. Eur. J. 11:1592
[69] Zener C (1932) Proc. R. Soc. A 137:696
[70] Wernsdorfer W, Bhaduri S, Vinslava A, Christou G (2005) Phys. Rev. B 72:4429
[71] Wernsdorfer W, Sessoli R (1999) Science 284:133
[72] Lecren L, Wernsdorfer W, Li Y-G, Roubeau O, Miyasaka H, Clérac R (2005) J. Am. Chem. Soc. 127:11311
[73] Wernsdorfer W, Bonet Orozco E, Hasselbach K, Benoit A, Barbara B, Demoncy N, Loiseau A (1997) Phys. Rev. Lett. 78:1791
[74] Wernsdorfer W, Murugesu M, Tasiopoulos T, Christou G (2005) Phys. Rev. B 72:212406
[75] Miyagawa K, Kanoda K, Kawamoto A (2004) Chem. Rev. 104:5635 and references therein